

Numerical Investigation of the Parabolic Mixed-Derivative Diffusion Equation via Alternating Direction Implicit Methods

Melisha Sathinarain

0410947D

Supervisor: Dr. C. Harley

Centre for Differential Equations, Continuum Mechanics and Applications
School of Computational and Applied Mathematics
University of the Witwatersrand
Private Bag 3, Wits 2050, Johannesburg, South Africa

May 14, 2013

Declaration

I declare that this dissertation is my own unaided work. It is being submitted for the degree of Master of Science at the University of the Witwatersrand, Johannesburg. It has not been submitted before for any degree or examination at any other university.

Melisha Sathinarain

May 14, 2013

Abstract

In this dissertation, we investigate the parabolic mixed derivative diffusion equation modeling the viscous and viscoelastic effects in a non-Newtonian viscoelastic fluid. The model is analytically considered using Fourier and Laplace transformations. The main focus of the dissertation, however, is the implementation of the Peaceman-Rachford Alternating Direction Implicit method. The one-dimensional parabolic mixed derivative diffusion equation is extended to a two-dimensional analog. In order to do this, the two-dimensional analog is solved using a Crank-Nicholson method and implemented according to the Peaceman-Rachford ADI method. The behaviour of the solution of the viscoelastic fluid model is analysed by investigating the effects of inertia and diffusion as well as the viscous behaviour, subject to the viscosity and viscoelasticity parameters. The two-dimensional parabolic diffusion equation is then implemented with a high-order method to unveil more accurate solutions. An error analysis is executed to show the accuracy differences between the numerical solutions of the general ADI and high-order compact methods. Each of the methods implemented in this dissertation are investigated via the von-Neumann stability analysis to prove stability under certain conditions.

Dedication

This masters dissertation is dedicated to all my family that supported me and believed in me. My mum and dad, who have inspired and motivated me to achieve everything I dream of. My brother and sister who never doubted me and my boyfriend who continuously supported me. This is especially dedicated to Jesus Christ, through whom I can do all things because He strengthens me.

Jeremiah 29:11 “For I know the plans I have for you”, says the Lord, “Plans to prosper you and not to harm you, plans to give you hope and a future”.

Acknowledgements

I would like to thank my supervisor Dr. C. Harley for all of her assistance, patience and especially for her ability to accommodate my demanding schedule during my MSc. Also, many thanks to Prof. E. Momoniat for his guidance. A special thanks to Prof. D. Mason for his assistance in investigating the physical significance of the fluid mechanics parameters, α and ν .

Contents

List of Figures	ix
List of Tables	x
1 Introduction	1
1.1 Derivation of the Mixed Derivative Diffusion Equation	2
1.2 Physical Significance of Parameters	5
1.2.1 Non-Newtonian Viscoelastic Fluids	10
1.2.2 Analytical and Graphical Interpretation of Parameters	12
2 Fourier and Laplace Transform Solutions	15
2.1 Fourier Transform Solutions to the Mixed Derivative Equation	15
2.2 Laplace Transform Solutions	18
3 Stability and Numerical Analyses	22
3.1 Derivation of the Difference Scheme for the Discrete One-Dimensional Equation	22
3.2 Von Neumann Stability Analysis	23
3.3 Numerical Analysis	25
4 Two-Dimensional Diffusion Equation	30

4.1	Derivation of the Discrete Two-Dimensional Diffusion Equation	30
4.2	Stability of the Two-Dimensional Equation	32
4.3	Peaceman-Rachford ADI Scheme with Crank-Nicholson	34
4.3.1	Accuracy of Scheme	34
4.3.2	Numerical Results	36
4.4	Physical Interpretation of Results	39
5	High-Order Compact ADI Method	47
5.1	Derivation of the High-Order Compact ADI Method for the Two-Parameter Mixed Derivative Equation	47
5.2	Stability Analysis	49
5.3	Numerical Analysis and Results	53
5.4	Comparative Study between the ADI and Compact ADI Methods	56
5.5	Physical Interpretation of Results	58
6	Conclusion	63
	Bibliography	66

List of Figures

1.1	A Boundary Layer (Source: Chhabra and Richardson, 2008)	6
1.2	Shearing Flow in One Direction (Source: Chhabra and Richardson, 2008) .	7
1.3	Shear-Stress Shear-Rate Relationship (Source: Chhabra and Richardson, 2008)	7
1.4	Viscosity Values at Room Temperature (Source: Chhabra and Richardson, 2008)	8
1.5	Three-Dimensional Flow Stress Components (Source: Chhabra and Richardson, 2008)	9
1.6	Examples of Non-Newtonian Substances (Source: Chhabra and Richardson, 2008)	10
1.7	Qualitative Differences Between a Viscous Fluid and an Elastic Solid (Source: Chhabra and Richardson, 2008)	11
2.1	Plot comparing the point source solution and the Fourier solution with $Dt = 1$ and $Dt = 2$	17
2.2	Plot comparing the point source solution and the Fourier solution with $\nu = 2$ and $\alpha = 10$	18
2.3	Plot comparing the Fourier solution and the numerical inversion of the Laplace transform solution for $D = 1$	21
2.4	Plot comparing the point source solution and the numerical inversion of the Laplace transform solution with $D = 1$, $\nu = 2$ and $\alpha = 10$	21

3.1	Plot of $u(x, t)$ when $\nu = 1$ and $\alpha = -1, 0, 1$	27
3.2	Individual plots of $u(x, t)$ when $\nu = 1$ and $\alpha = -1, 0, 1$ and the initial profile.	27
3.3	Plot of $u(x, t)$ when $\nu = 1$ and $\alpha = -10, 0, 1$	28
4.1	Plot of the Initial Profile $u(x, y, t) = e^{(x^2-y^2)}$ at $t=0$	39
4.2	Plot of $u(x, y, t)$ for $\alpha = 0$ and $\nu = 1$ and for $\alpha = 1$ and $\nu = 1$	40
4.3	Plot of $u(x, y, t)$ displaying diffusion effects for $\alpha = 0$ and $\nu = 2$ and for $\alpha = 0$ and $\nu = 4$	41
4.4	Plot of $u(x, y, t)$ displaying diffusion effects for $\alpha = 0$ and $\nu = 6$ and for $\alpha = 0$ and $\nu = 9$	42
4.5	Plot of $u(x, y, t)$ displaying viscoelastic effects for $\alpha = 1$ and $\nu = 9$ and for $\alpha = 2$ and $\nu = 9$	43
4.6	Plot of $u(x, y, t)$ displaying viscoelastic effects for $\alpha = 3$ and $\nu = 9$ and for $\alpha = 5$ and $\nu = 9$	44
4.7	Plot of $u(x, y, t)$ for $\alpha = 5$ and $\nu = 2$ and for $\alpha = 6$ and $\nu = 3$	45
5.1	Plot of $u(x, y, t)$ of the Compact ADI method at $\alpha = 0$ and $\nu = 1$ and for $\alpha = 1$ and $\nu = 1$	55
5.2	Plot of the absolute error between the numerical solution obtained via the ADI method and the numerical solution obtained via the compact ADI method for $\Delta t = 0.05$ and $N = 100$	56
5.3	Plot of the log of the absolute error between the numerical solution obtained via the ADI method and the numerical solution obtained via the compact ADI method for $\Delta t = 0.05$ and $N = 100$	57
5.4	Plot of the infinity norm of the numerical solution obtained via the ADI method and the numerical solution obtained via the compact ADI method for $\Delta t = 0.05$ and $N = 100$	57
5.5	Plot of $u(x, y, t)$ displaying diffusion effects of the Compact ADI method at $\alpha = 0$ and $\nu = 3$ and for $\alpha = 0$ and $\nu = 5$	59

5.6	Plot of $u(x, y, t)$ displaying diffusion effects of the Compact ADI method at $\alpha = 0$ and $\nu = 7$	60
5.7	Plot of $u(x, y, t)$ displaying viscoelastic effects of the Compact ADI method at $\alpha = 1$ and $\nu = 7$	60
5.8	Plot of $u(x, y, t)$ displaying viscoelastic effects for $\alpha = 3$ and $\nu = 7$ and for $\alpha = 5$ and $\nu = 7$	61
5.9	Plot of $u(x, y, t)$ displaying viscoelastic effects of the Compact ADI method at $\alpha = 50$ and $\nu = 7$	62

List of Tables

1.1	Reynolds Number Values and Effect on the Physical Behaviour of the Fluid	13
6.1	Summary of the behaviour of the parameters as a result of the general ADI numerical solutions	64
6.2	Summary of the behaviour of the parameters as a result of the compact ADI numerical solutions	65

Chapter 1

Introduction

Various authors have investigated a range of one-parameter mixed derivative diffusion equations. Momoniat [1], has done recent work on Cattaneo's [2] equation which has a single parameter, D given by $D = \frac{\nu}{\alpha}$ where ν represents kinematic viscosity and α represents viscoelasticity. Cattaneo's equation has been analysed for $Dt \ll 1$ as well as their zeroth, first and second moments, by Momoniat [1, 3] in which he showed that a one-parameter parabolic mixed derivative diffusion equation reveals certain statistical similarities with those of the phenomenological diffusion equation.

Momoniat [3] showed that for $Dt \ll 1$, the second moment of the approximation of $u(x, t)$ suggests that the fluid undergoes anomalous diffusion classified as superdiffusion. This is proven otherwise by Wafo Soh [4] by performing exact computations of the moments. As a consequence of this analysis Wafo Soh discovers that the average relaxation time τ is $\frac{1}{D}$ [4].

Momoniat and Harley [5] investigated a one-parameter mixed derivative diffusion equation as well as its two-dimensional analog that is representative of the two-dimensional flow of a second grade fluid. They prove that the approach adopted in their investigation is easier to implement than the traditional homotopy analysis and homotopy perturbation methods that are generally used to find numerical solutions for equations modelling the flow of higher grade fluids.

The parabolic mixed derivative diffusion equation with the two separate parameters of ν and α have not been previously investigated and as such is the focus of this dissertation. Moreover, we obtain more numerically accurate solutions, that is, 6^{th} order accurate solutions for this two-parameter equation via a method which has not previously been implemented on this problem.

In this dissertation we will investigate the two-parameter parabolic mixed derivative diffu-

sion equation for different parameter values of the kinematic viscosity, ν and viscoelasticity, α . The one-dimensional two parameter mixed derivative diffusion equation will be considered and analysed via Fourier and Laplace transform solutions. This analysis sets the behavioural expectation resulting from the implementation of the Peaceman-Rachford ADI method on the one-dimensional equation.

The one-dimensional two-parameter mixed derivative diffusion equation is then extended to the two-dimensional analog and implemented via the Peaceman-Rachford ADI method. The equation is solved by the Crank-Nicholson method. The two-dimensional analog is implemented with higher accuracy using the compact ADI method. The behaviour of these solutions will be investigated for different values of viscosity and viscoelasticity to display diffusion, viscoelastic and inertial effects. The consistency of the results across all methods for the one- and two-dimensional versions of the two-parameter mixed derivative diffusion equation will be considered.

The two-parameter mixed derivative diffusion equation which is the main focus of this dissertation, will be derived in the section to follow.

1.1 Derivation of the Mixed Derivative Diffusion Equation

The simplest of the rheological models for second grade viscoelastic fluids was found by Rivlin and Ericksen [6]. Here we will derive a model that will be the focus of this dissertation, the parabolic mixed derivative diffusion equation which models the unidirectional flow of a viscoelastic fluid is given by,

$$\frac{\partial u}{\partial t} - D \frac{\partial^2 u}{\partial x^2} - \frac{\partial^3 u}{\partial t \partial x^2} = 0, \quad (1.1)$$

where D is the ratio of kinematic viscosity (ν) and viscoelasticity (α), $D = \nu/\alpha$. A viscoelastic fluid displays both viscous and elastic properties. The fluid considered here is modelled as a second grade fluid and hence classed as a higher grade fluid [1]. This type of fluid cannot adequately be described by the classical Newtonian model, hence the incompressible second grade fluid model is implemented instead [7].

Rajagopal [7] derived this equation by considering the stress tensor \mathbf{T} in a non-Newtonian second grade fluid which is given by the constitutive equation,

$$\mathbf{T} = -p\mathbf{I} + \mu\mathbf{A}_1 + \beta_1\mathbf{A}_2 + \beta_2\mathbf{A}_1^2, \quad (1.2)$$

where $\alpha = \beta_1/\rho$ and $\nu = \mu/\rho$ are constants, μ is the coefficient of fluid viscosity, ρ is the fluid density, ν is the kinematic viscosity and $-p\mathbf{I}$ is the indeterminate spherical stress tensor with p the pressure in the fluid. β_1 and β_2 are the normal stress moduli of the fluid, specifically β_1 represents viscoelasticity, a non-Newtonian fluid parameter, and β_2 the cross-viscosity term. Equation (1.1), also derived and analysed by Hayat et al. [8], models transient flows of a non-Newtonian second grade fluid.

The kinematic stress tensors are given by the following equations,

$$\mathbf{A}_1 = (\text{grad}\mathbf{V}) + (\text{grad}\mathbf{V})^T, \quad (1.3)$$

$$\mathbf{A}_2 = \frac{d}{dt}\mathbf{A}_1 + \mathbf{A}_1(\text{grad}\mathbf{V}) + (\text{grad}\mathbf{V})^T\mathbf{A}_1, \quad (1.4)$$

where \mathbf{V} is the velocity, grad is the gradient, and $\frac{d}{dt}$ is the material time derivative. The balance of linear momentum is given by,

$$\text{div}\mathbf{T} + \rho\mathbf{b} = \rho\frac{d\mathbf{V}}{dt}, \quad (1.5)$$

where \mathbf{b} is the conservative body force field. We assume a zero body force and the incompressibility of the fluid. The unsteady motion of the fluid is therefore modelled by the resulting two equations [1],

$$\text{div}\mathbf{V} = 0, \quad (1.6)$$

$$\rho\frac{d\mathbf{V}}{dt} = \text{div}\mathbf{T}. \quad (1.7)$$

Upon substitution of equations (1.2), (1.3) and (1.4) into equation (1.7), one obtains,

$$\begin{aligned} \rho\frac{d\mathbf{V}}{dt} &= \text{div}(-p\mathbf{I}) + \mu\text{div}(\text{grad}\mathbf{V} + (\text{grad}\mathbf{V})^T) \\ &\quad + \beta_1(\text{div}(\frac{d}{dt}(\text{grad}\mathbf{V} + (\text{grad}\mathbf{V})^T)) + \text{div}\mathbf{A}_1(\text{grad}\mathbf{V}) + \text{div}(\text{grad}\mathbf{V})^T\mathbf{A}_1) \\ &\quad + \beta_2(\text{div}(\text{grad}\mathbf{V} + (\text{grad}\mathbf{V})^T)^2). \end{aligned} \quad (1.8)$$

By assuming unidirectional flow, that is $\mathbf{V} = (u(x, t), 0, 0)$, ignoring pressure gradients and considering equation (1.6) reduces equation (1.8) to the partial differential equation,

$$\frac{\partial u}{\partial t} - \nu \frac{\partial^2 u}{\partial x^2} - \alpha \frac{\partial^3 u}{\partial t \partial x^2} = 0, \quad (1.9)$$

which is the form of equation (1.1) which we will predominantly be considering. Equation (1.1) is obtained by applying the transformation,

$$x \rightarrow \sqrt{\alpha x}. \quad (1.10)$$

When the following transformations are applied,

$$t \rightarrow -\bar{t}, \quad x \rightarrow i\bar{x}, \quad u \rightarrow -\bar{u}, \quad (1.11)$$

equation (1.1) becomes the equation derived by Cattaneo [2]. Cattaneo considered the history of the temperature gradient on the heat flux arriving at the equation,

$$\frac{\partial u}{\partial t} - D \frac{\partial^2 u}{\partial x^2} + \frac{\partial^3 u}{\partial t \partial x^2} = 0. \quad (1.12)$$

This equation predicts the diffusion of point sources with infinite speed and was therefore of no further importance to Cattaneo [2]. The further analysis of equation (1.12) done by Momoniat [9] will be discussed later. At a later stage comparisons will also be made to the phenomenological diffusion equation given by [10],

$$\frac{\partial u}{\partial t} - D \frac{\partial^2 u}{\partial x^2} = 0, \quad (1.13)$$

which, similar to Cattaneo's equation, also predicts the diffusion of a point source with infinite speed. In an attempt to eliminate the property of instantaneous heat conduction, as is relevant for the previous two equations, Cattaneo [2, 11] derived the equation known as the telegraph equation,

$$\frac{\partial u}{\partial t} + \tau \frac{\partial^2 u}{\partial t^2} = \frac{\partial^2 u}{\partial x^2}, \quad (1.14)$$

where τ is a constant known as the relaxation time.

The differential model (1.1) has various application in statistics, finance [4] and transient flows of higher grade fluids within fluid mechanics [1, 7, 8] and the transformed differential equation (1.12) models diffusion processes [2, 11, 3].

The telegraph equation, when modified with respect to the relaxation time τ , allows it to model a more realistic heat conduction process. This model has applications in fluid mechanics and diffusion processes [2, 11, 3]. A one parameter version of the two-parameter two dimensional model (4.1) considered by Momoniat [12] for $\kappa = 1$, is useful in modelling problems within statistics and financial mathematics.

In the following section, the physical significance of the main parameters, α and ν , will be discussed.

1.2 Physical Significance of Parameters

A number of authors have carried out interesting work with significant physical application to viscoelastic fluids in topics such as two-dimensional second grade fluids, unsteady unidirectional flows of non-Newtonian fluids and boundary layer flow.

Girault and Scott [13], analyse the two-dimensional second grade fluid according to tangential boundary conditions. It was found that each solution of the second-grade fluid model satisfies energy equalities and converges to the solution of the Navier-Stokes equations when the normal stress modulus of the fluid tends to zero.

I-Chung Liu [14] investigates the unsteady unidirectional flows of a non-Newtonian fluid saturated in a porous medium as well as flows caused by an oscillatory pressure gradient and surfaces oscillating in their own planes. It was found, most importantly, apart from the retardation effects on the flow of the magnetic field and the porous medium, that the viscoelastic effects of the second grade fluid on the behaviour of the flow is complicated.

Damseh, Shatnawi, Chamkha and Duwairi [15] analyse viscoelastic boundary flow by numerically solving the governing equations of the problem. They analyse the behaviour of the velocity temperature profiles, boundary layer thickness, Nusselt numbers and friction coefficients for various values of the viscoelastic parameter. They found that the velocity within the boundary layer decreases as the viscoelastic parameter is increased.

For Newtonian fluids, inviscid fluid theory fails to take into consideration the effects of a boundary layer. A boundary layer is evidence that there is no such slip of the fluid in contact with an aerofoil, however the fluid in contact with the aerofoil reaches a velocity of zero, suggesting a thin layer of fluid with no slip. In this boundary layer, viscous effects are evident. Consider the case of shear flow $\mathbf{u} = [u(y), 0, 0]$ and Figure 1.1. Above a constant level, y , the fluid exerts a stress. Viscous fluids have a non-zero tangential element, τ , to this stress, whereas inviscid fluids do not [16].

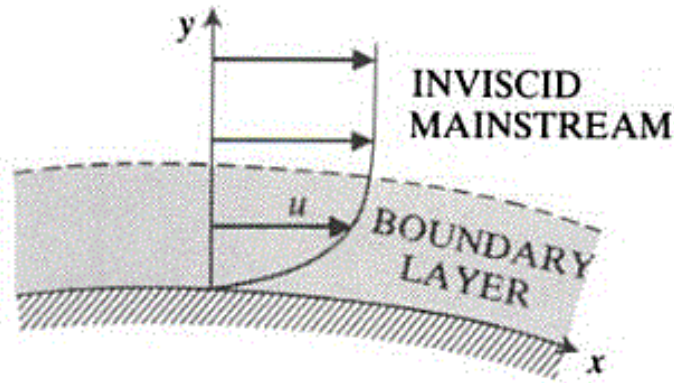


Figure 1.1: *A Boundary Layer (Source: Chhabra and Richardson, 2008)*

Batchelor [17] makes reference to an example of transportation of momentum in simple shearing motion to describe the effect of viscosity. A simple shearing motion is a motion in which planes, located parallel to the surface element exhibit a rigid sliding motion over each other. If the fluid velocities on either side of the surface elements are different, molecular motion between the elements will tend to occur to eliminate the presence of the velocity differences. This resulting transport of momentum, is actually internal friction. A fluid exhibiting such an internal friction is said to be viscous.

It is imperative to demonstrate this characteristic behaviour in Newtonian fluids, in order to classify the behaviour of non-Newtonian fluids. Chhabra and Richardson [18] give details on the classification of a Newtonian fluid and when the fluids are non-Newtonian.

There are two ways to classify the behaviour of a fluid. One is by considering its behaviour when a pressure is applied to it, which defines whether a fluid is compressible or incompressible. The other is to classify a fluid under the effects of shear stress.

Consider a thin fluid layer between two parallel plates that are a distance, dy apart, as in Figure 1.2.

Assuming steady state conditions, an application of a shearing force F produces an equal and opposite internal friction in the fluid to maintain the steady state. In [18] the shear rate is expressed as the velocity gradient, $-\frac{dV_x}{dy}$, perpendicular to the shear force for an incompressible Newtonian fluid in laminar flow.

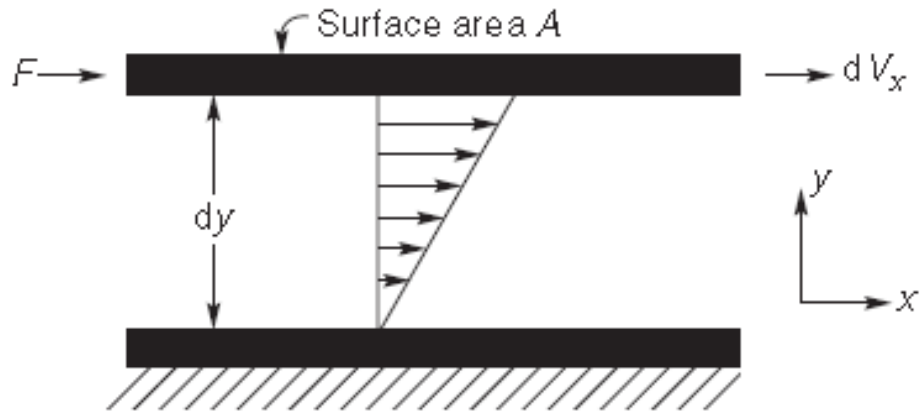


Figure 1.2: *Shearing Flow in One Direction* (Source: Chhabra and Richardson, 2008)

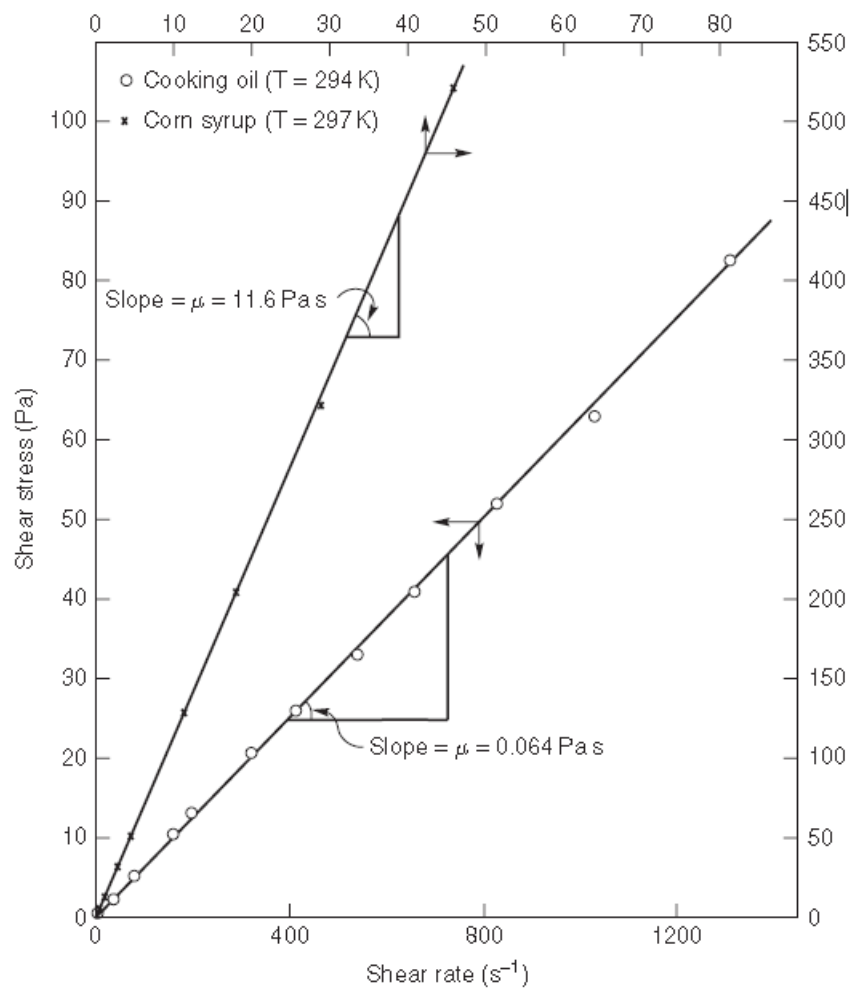


Figure 1.3: *Shear-Stress Shear-Rate Relationship for Cooking Oil and Corn Syrup* (Source: Chhabra and Richardson, 2008)

This relationship of the shear rate $\dot{\gamma}_{yx}$ is given by,

$$\tau_{yx} = \frac{F}{A} = \nu \left(-\frac{dV_x}{dy} \right) = \nu \dot{\gamma}_{yx}. \quad (1.15)$$

This equation shows that the shear stress is the product of the viscosity and the shear rate of the fluid. In equation (1.15) the direction of the shear stress τ_{yx} is opposite to the direction of the motion of the fluid, therefore it is a measure of resistance to the motion of the fluid.

For an incompressible fluid with density, ρ , equation (1.15) can be written as,

$$\tau_{yx} = -\frac{\nu}{\rho} \frac{d}{dy}(\rho V_x), \quad (1.16)$$

where ρV_x is the linear momentum per unit volume of the fluid, in the x-direction, therefore, τ_{yx} is the momentum flux in the y-direction. The momentum transfer occurs in the direction of decreasing velocity. The viscosity, ν , is independent of the shear stress (τ_{yx}), or shear rate ($\dot{\gamma}_{yx}$), but it is dependent on the material and its temperature and pressure [18].

The plot of shear stress and shear strain, for a Newtonian fluid is a straight line with a slope of ν . This slope passes through the origin. Therefore ν fully characterises the behaviour of a Newtonian fluid at constant temperature and pressure.

Substance	μ (mPas)
Air	10^{-2}
Benzene	0.65
Water	1
Molten sodium chloride (1173 K)	1.01
Ethyl alcohol	1.20
Mercury (293 K)	1.55
Molten lead (673 K)	2.33
Ethylene glycol	20
Olive oil	100
Castor oil	600
100% Glycerine (293 K)	1500
Honey	10^4
Corn syrup	10^5
Bitumen	10^{11}
Molten glass	10^{15}

Figure 1.4: *Viscosity Values at Room Temperature (Source: Chhabra and Richardson, 2008)*

The diagram in Figure 1.3, shows the relationship between shear stress and shear strain for cooking oil and corn syrup [18]. Chhabra [19] provides a table of the viscosities of substances held at room temperature in Figure 1.4.

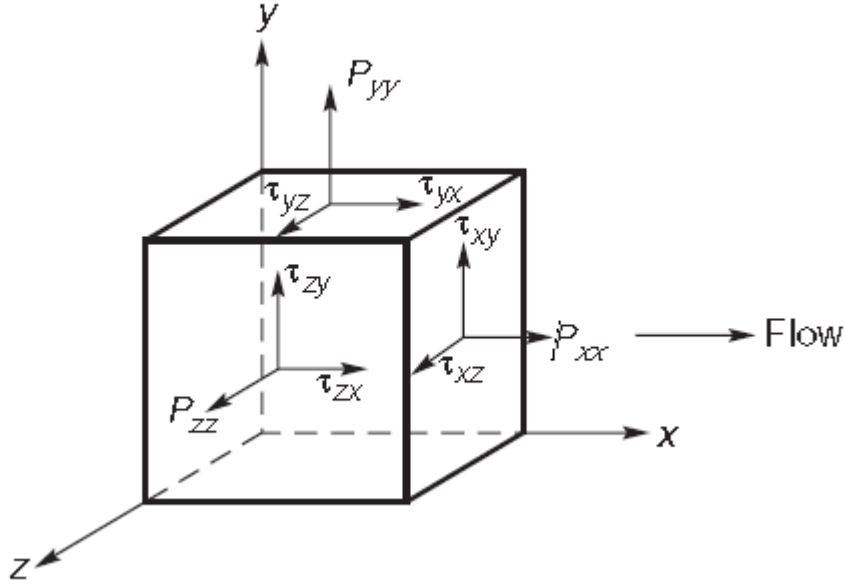


Figure 1.5: *Three-Dimensional Flow Stress Components* (Source: Chhabra and Richardson, 2008)

Take into consideration the stress components in a three-dimensional flow space as per Figure 1.5. The definition of a simple shearing Newtonian fluid satisfies the condition of constant viscosity and the condition,

$$\tau_{xx} = \tau_{yy} = \tau_{zz} = 0, \quad (1.17)$$

that is, a Newtonian fluid satisfies the full set of Navier-Stokes equations.

A fluid, that does not satisfy either condition, is classified as a non-Newtonian fluid. Chhabra and Richardson [18] give a table of examples in Figure 1.6 of these kinds of fluids that occur in everyday life.

1.2.1 Non-Newtonian Viscoelastic Fluids

Chhabra and Richardson [19] describe Non-Newtonian fluid behaviour to be one where the flow curve, that is, shear stress versus shear rate, is non-linear or does not pass through the origin. This means that the viscosity which is shear stress divided by shear strain is not constant at a given temperature and pressure but is dependent on flow conditions such as flow geometry and shear rate. This can also be dependent on the kinematic history of the fluid element. Chhabra and Richardson class these fluids into three types [18]. The first class of fluids are known as ‘time-independent’, ‘purely viscous’, ‘inelastic’, or ‘generalized Newtonian fluids (GNF)’. The shear rate for these fluids at any point is determined only by the value of the shear stress at that point, at that instant in time. The second class are ‘time-dependent’ fluids. They are more complex substances where the relation between shear rate and shear stress have additional dependencies upon the duration of shearing and their kinematic history. The third class of fluids are viscoelastic fluids categorised to be substances that display both the characteristics of ideal fluids and elastic solids, where after deformation they exhibit partial elastic recovery [18].

Most materials exhibit more than one or all of these characteristics, however, the dominant non-Newtonian characteristic can be determined [18]. For the purposes of this dissertation a further discussion on viscoelastic fluids will be addressed.

■ Adhesives (wall paper paste, carpet adhesive, for instance)	■ Foodstuffs (fruit/vegetable purees and concentrates, sauces, salad dressings, mayonnaise, jams and marmalades, ice-cream, soups, cake mixes and cake toppings, egg white, bread mixes, snacks)
■ Ales (beer, liqueurs, etc.)	■ Greases and lubricating oils
■ Animal waste slurries from cattle farms	■ Mine tailings and mineral suspensions
■ Biological fluids (blood, synovial fluid, saliva, etc.)	■ Molten lava and magmas
■ Bitumen	■ Paints, polishes and varnishes
■ Cement paste and slurries	■ Paper pulp suspensions
■ Chalk slurries	■ Peat and lignite slurries
■ Chocolates	■ Polymer melts and solutions, reinforced plastics, rubber
■ Coal slurries	■ Printing colours and inks
■ Cosmetics and personal care products (nail polish, lotions and creams, lipsticks, shampoos, shaving foams and creams, toothpaste, etc.)	■ Pharmaceutical products (creams, foams, suspensions, for instance)
■ Dairy products and dairy waste streams (cheese, butter, yogurts, fresh cream, whey, for instance)	■ Sewage sludge
■ Drilling muds	■ Wet beach sand
■ Fire fighting foams	■ Waxy crude oils

Figure 1.6: *Examples of Non-Newtonian Substances (Source: Chhabra and Richardson, 2008)*

Viscoelastic Fluids

Viscoelastic fluids will be the focus of this dissertation given that the parabolic mixed-derivative equation models a viscoelastic fluid where the presence of the viscoelastic fluid parameters indicates as much. A viscoelastic fluid is one that exhibits both viscous and elastic effects. A material is elastic if after distortion, it returns to its original shape. However for a solid when the applied stress exceeds the yield stress of the material, ‘creep’ will occur instead of complete recovery, that is, the solid would have flowed [18]. A viscous fluid is one that exhibits a resistance to shear or tensile stress.

The two viscoelastic fluid parameters of main consideration in this dissertation are ν , the kinematic viscosity and α the viscoelasticity. Kinematic viscosity, ν , is defined as $\frac{\mu}{\rho}$ and viscoelasticity, α , is defined as $\frac{\beta_1}{\rho}$ where μ is the coefficient of the fluid viscosity, ρ the fluid density and β_1 represents the normal stress moduli of the fluid.

Weissenberg [20] was the first to discover that unequal normal stresses are present in viscoelastic fluids undergoing a shearing motion. Hence, the normal stress moduli is an important consideration when observing viscoelasticity of a fluid.

The Non-Newtonian fluids in question are those whose viscosities change with a change in the strain rate on the fluid.

In practice, it is not unusual that a viscoelastic material could behave as a viscous fluid under certain conditions, and as an elastic solid under different conditions. Common materials found in practice, such as, polymer melts, polymer and soap solutions and synovial fluid (a Non-Newtonian fluid found in the synovial joint of the human body), exhibit viscoelastic behaviour. These materials have some ability to store and recover shear energy as shown in Figure 1.7 [18].

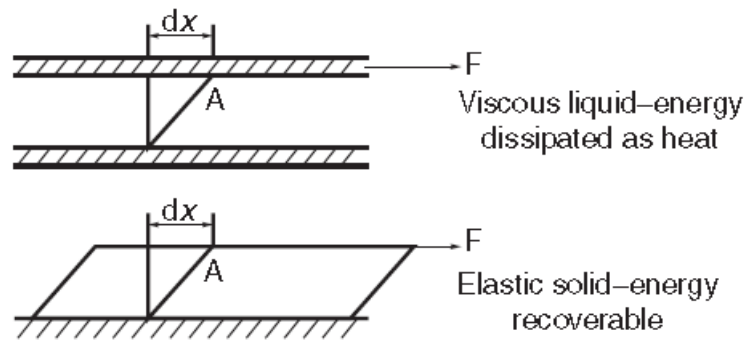


Figure 1.7: *Qualitative Differences Between a Viscous Fluid and an Elastic Solid (Source: Chhabra and Richardson, 2008)*

1.2.2 Analytical and Graphical Interpretation of Parameters

This section shows the typical behaviour of the parameters of viscosity and inertia referred to in this dissertation according to the quantifiable laws of Newtonian fluids.

Substitute into equation (1.9) the following,

$$t = \bar{t}T,$$

$$x = \bar{x}L$$

and

$$u = \bar{u}U. \quad (1.18)$$

Also since U represents the speed of the flow, and L is the characteristic length scale of the flow, we find that $T = \frac{L}{U}$ and therefore we have the result,

$$\frac{\partial \bar{u}}{\partial \bar{t}} - \frac{\nu}{UL} \frac{\partial^2 \bar{u}}{\partial \bar{x}^2} - \frac{\alpha}{L^2} \frac{\partial^3 \bar{u}}{\partial \bar{t} \partial \bar{x}^2} = 0. \quad (1.19)$$

Given that Reynolds number is a pure number given by $Re = \frac{UL}{\nu}$, the ratio of the inertia effects to the viscous effects, therefore (1.19) becomes,

$$\frac{\partial \bar{u}}{\partial \bar{t}} - \frac{1}{Re} \frac{\partial^2 \bar{u}}{\partial \bar{x}^2} - \frac{\alpha}{L^2} \frac{\partial^3 \bar{u}}{\partial \bar{t} \partial \bar{x}^2} = 0. \quad (1.20)$$

Subsequently, a high Reynolds number flow exhibits very different characteristics to that of a low Reynolds number flow.

Case 1: Reynolds Number

Since $Re = \frac{UL}{\nu}$, for a large Reynolds Number, that is, for $Re \gg 1$, the coefficient $\left(\frac{1}{\frac{UL}{\nu}}\right)$ is approximately 0, therefore $\left(\frac{\nu}{UL}\right) \approx 0$. Hence, since the ratio $\frac{\nu}{UL} = \frac{\text{viscous effects}}{\text{inertia effects}}$, the viscous effects are not significant here, rendering the spatial derivative in the x-direction of the second term of equation (1.20) to have negligible effects on the results. Also, the effects of inertia are more dominant than viscous effects.

When $Re \ll 1$, $\frac{1}{Re} \gg 1$ which in turn implies that $\frac{UL}{\nu} \ll 1$. Hence $UL \ll \nu$ which reveals that the viscous effects are more dominant as opposed to the inertial effects.

Case 2: Viscoelastic Effects

The viscoelastic effects are significant if the coefficient of the mixed derivative term in equation (1.9) is much greater than that of the spatial derivative. Hence, since the condition is $\frac{\alpha}{L^2} \gg \frac{1}{Re}$, $\frac{L^2}{\alpha} \ll Re$ is required for the viscoelastic effects to dominate.

Table 1.1 summarises the relationship between the behaviour of the terms in the equation.

	Condition	Relationship
1.	$Re \gg 1$	Viscous effects are negligible in the results
2.	$Re \ll 1$	When the Reynolds number is negligible the results exhibit slow viscous flow
3.	$Re \gg \frac{L^2}{\alpha}$	Viscoelastic effects are important and significantly effect results

Table 1.1: Reynolds Number Values and Effect on the Physical Behaviour of the Fluid

The effect of increased values of ν on the spatial derivative is diffusion, a process that causes the solitary wave to broaden. This broadening also causes a lower amplitude on the wave hence a lower profile height. However, increased values of the viscoelastic coefficient on the mixed derivative term, causes oscillations which oppose broadening of the profile. Another interesting observation, which will be shown graphically later, is the effect of the boundary conditions, $\frac{\partial u}{\partial x} \approx 0$ and $\frac{\partial u}{\partial y} \approx 0$. For very large values of ν and α , and an increased domain and range on the profile, there is some sort of disturbance that occurs at the boundaries.

The behaviour due to diffusion can be quantified in itself, ignoring the viscoelastic effects, hence ignoring the mixed derivative term, as follows,

$$\frac{\partial u}{\partial t} = \nu \frac{\partial^2 u}{\partial x^2}.$$

Using the substitutions (1.18), the dimensions of the standard diffusion equation above reduces to,

$$L = (\nu T)^{\frac{1}{2}},$$

which represents the distance diffused in time T and

$$T = \frac{L^2}{\nu},$$

representing the time taken to diffuse a distance L .

Later in this dissertation, the effects of diffusion on the solutions will be considered, ignoring the viscoelastic effects. Lastly it is important to note that the numerical values chosen for the parameters α and ν relate to various practical applications; one such application is for instance bio-fluids where synovial fluid being a particular example of a viscoelastic fluid [19]. Furthermore, the values of the parameters are chosen so as to demonstrate the numerical effects of the solution.

Chapter 2

Fourier and Laplace Transform Solutions

In this section Fourier transform solutions of the mixed derivative equation (1.1) and the phenomenological diffusion equation (1.13) are found as done by Momoniat [1]. Comparisons are drawn between their respective numerically evaluated solutions [1]. A Laplace transform solution of equation (1.12) with $D = 1$ is obtained and analysed [9]. These methods are subsequently applied to the two-parameter parabolic mixed derivative diffusion equation (1.9) which incorporates the parameters of kinematic viscosity and viscoelasticity.

2.1 Fourier Transform Solutions to the Parabolic Mixed Derivative Diffusion Equation

The equations being considered in this section are the phenomenological diffusion equation (1.13),

$$\frac{\partial u}{\partial t} - D \frac{\partial^2 u}{\partial x^2} = 0, \quad (2.1)$$

and the mixed derivative equation (1.1),

$$\frac{\partial u}{\partial t} - D \frac{\partial^2 u}{\partial x^2} - \frac{\partial^3 u}{\partial t \partial x^2} = 0. \quad (2.2)$$

The analytical solutions of these equations are first considered in order to compare them to the subsequent numerical Fourier transform solutions and justify the numerical results

obtained. In the first part of this section, the work by Momoniat [1] is reproduced in order to check the methodology which we will apply to our parabolic mixed derivative diffusion equation, later on in this section.

The point source solution of the phenomenological diffusion equation (1.13) is well known [10],

$$u(x, t) = \frac{1}{\sqrt{4\pi Dt}} \exp\left(-\frac{x^2}{4Dt}\right). \quad (2.3)$$

By substituting the Fourier integral into equation (1.1) we obtain,

$$u(x, t) = \frac{1}{2\pi} \int_{-\infty}^{\infty} f(k, t) \cos(kx) dk, \quad (2.4)$$

with $f(k, t)$ emerging as $\exp\left(-\frac{k^2 Dt}{1+k^2}\right)$ to give the solution,

$$u(x, t) = \frac{1}{2\pi} \int_{-\infty}^{\infty} \exp\left(-\frac{k^2 Dt}{1+k^2}\right) \cos(kx) dk. \quad (2.5)$$

The behaviour of the exponential function is the characteristic determining the boundedness of the integral (2.5). Momoniat [1] reveals an asymptote at $k \in (-\infty, \infty)$ allowing for the boundedness of the integral. By considering the geometric series of the exponent and through the use of the Taylor series expansion for $e^{(\cdot)}$, the exponential function $f(k, t)$ can be simplified as follows,

$$\begin{aligned} \exp\left(-\frac{k^2 Dt}{1+k^2}\right) &= \exp(-k^2 Dt) \exp\left(\frac{k^4 Dt}{1+k^2}\right) \\ &\approx \exp(-k^2 Dt)(1 + k^4 Dt), \end{aligned} \quad (2.6)$$

which results in,

$$u(x, t) = \frac{1}{2\pi} \int_{-\infty}^{\infty} \exp(-k^2 Dt)(1 + k^4 Dt) \cos(kx) dk. \quad (2.7)$$

After further evaluation of the integral with the use of MATHEMATICA the resulting solution is,

$$u(x, t) \approx \frac{1}{32\sqrt{\pi D^9 t^7}} \exp\left(-\frac{x^2}{4Dt}\right) [4(Dt)^2(3 + 4D^2t) - 12Dtx^2 + x^4]. \quad (2.8)$$

By comparing the solutions (2.3) and (2.8), it is notable that we obtain similar results to Momoniat [1], where the solution of the mixed derivative diffusion equation (1.1) tends to the solution of the phenomenological diffusion equation (1.13) for $Dt \gg 1$.

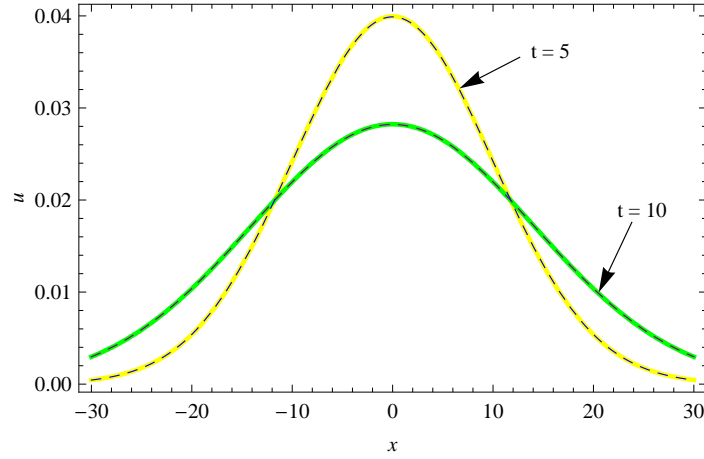


Figure 2.1: Plot comparing the point source solution of the phenomenological diffusion equation (2.3) (---) and the Fourier solution obtained for the mixed derivative equation (2.8) (___) with $Dt = 1$ and $Dt = 2$.

We now employ the same method used above to analyse the two-parameter mixed derivative diffusion equation (1.9),

$$\frac{\partial u}{\partial t} - \nu \frac{\partial^2 u}{\partial x^2} - \alpha \frac{\partial^3 u}{\partial t \partial x^2} = 0, \quad (2.9)$$

which is of main interest. After substitution of the Fourier integral (2.4) we obtain,

$$u(x, t) = \frac{1}{2\pi} \int_{-\infty}^{\infty} \exp\left(\frac{-\nu k^2 t}{(1 + \alpha k^2)}\right) \cos(kx) dk. \quad (2.10)$$

In a similar fashion we are able to write,

$$\begin{aligned} \exp\left(\frac{-\nu k^2 t}{(1 + \alpha k^2)}\right) &= \exp(-\nu k^2 t) \exp\left(\frac{-\nu \alpha k^4 t}{1 + \alpha k^2}\right) \\ &\approx \exp(-\nu k^2 t)(1 + \nu \alpha k^4 t), \end{aligned} \quad (2.11)$$

such that,

$$u(x, t) \approx \frac{1}{\sqrt{8\pi\nu^7}} \exp\left(-\frac{x^2}{8\nu}\right) \left[\frac{(\alpha x^4 - 24\alpha\nu x^2 + 16\nu^2(3\alpha + 8\nu))}{128} \right], \quad (2.12)$$

with the use of MATHEMATICA.

It is evident from Figure 2.2 that the behaviour of $u(x, t)$ is similar to that of the solution (2.8) obtained for equation (1.1). However we notice that $u(x, t)$ exhibits increased oscillation until it eventually dampens out as previously encountered for the solution given by (2.8).

2.2 Laplace Transform Solutions

In a paper by Momoniat, McIntyre and Ravindran [9] the Laplace transform of equation (1.12) with $D = 1$ is considered. This is motivated by the instability of the Method of Lines when applied to this differential equation. The Method of Lines is proved to be stable

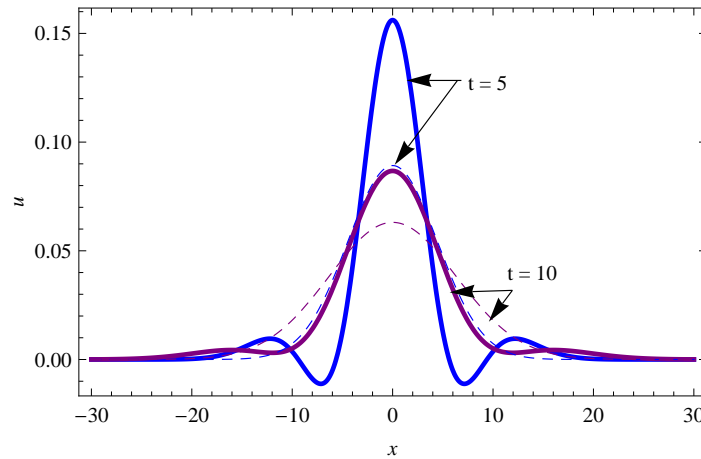


Figure 2.2: Plot comparing the point source solution for the phenomenological diffusion equation (2.3) (---) and the Fourier solution obtained for the two-parameter mixed derivative equation (2.12) (___) with $\nu = 2$ and $\alpha = 10$.

for the numerical analysis of the mixed derivative equation (1.1) and the phenomenological diffusion equation (1.13) both for $D = 1$ [9]. In this section we will consider the stable Laplace transform solution of equation (1.12),

$$\frac{\partial u}{\partial t} - D \frac{\partial^2 u}{\partial x^2} + \frac{\partial^3 u}{\partial t \partial x^2} = 0, \quad (2.13)$$

with $D = 1$ and by implementing the same method we will produce results for the two-parameter mixed derivative equation (1.9).

The Neumann and Dirichlet boundary conditions that describe equation (1.12) for $D = 1$ are,

$$\frac{\partial u}{\partial x}|_{x=0} = 0, \quad (2.14)$$

$$u(\infty, t) = 0, \quad (2.15)$$

and the diffusion of an initial point source is given by,

$$u(x, 0) = f(x) = \delta(x), \quad (2.16)$$

where $\delta(x)$ is the usual delta function which is considered as,

$$\delta_\eta(x) = \frac{1}{\eta\sqrt{\pi}} \exp\left(-\frac{x^2}{\eta^2}\right), \quad (2.17)$$

with,

$$\delta(x) = \lim_{\eta \rightarrow 0} \delta_\eta(x). \quad (2.18)$$

At $x = 0$, the Neumann boundary condition ensures that across the vertical axis the solution is continuous [9].

The Laplace Transform $\tilde{f}(s)$ of $f(t)$ is defined as,

$$\mathcal{L}[f(t)] = \tilde{f}(s) = \int_0^\infty \exp(-st) f(t) dt \quad \text{for } s > 0. \quad (2.19)$$

The Laplace transform is taken with respect to time, t ,

$$\mathcal{L} \left[\frac{\partial u}{\partial t} - D \frac{\partial^2 u}{\partial x^2} + \frac{\partial^3 u}{\partial t \partial x^2} \right] (s) = 0, \quad (2.20)$$

resulting in a second-order ordinary differential equation,

$$(s - D)F''(x) + sF(x) - f(x) - f''(x) = 0, \quad (2.21)$$

where $f(x)$ and $f''(x)$ refers to the initial condition (2.16) and it's second derivative respectively.

The boundary conditions (2.14) and (2.15) become,

$$F'(0) = 0, \quad F(\infty) = 0. \quad (2.22)$$

Equation (2.21) is solved using MATHEMATICA by implementing the function **NDsolve**. The solution to equation (1.12) with $D = 1$ is found by taking the inverse Laplace transform of F . This numerical inverse Laplace transform is difficult to compute analytically. We turn to an algorithm developed by Crump [21] for the numerical implementation of the inverse Laplace transform which will be applied here. This leads to the following inverse Laplace transform solution of F ,

$$u(x, t) = \frac{1}{2\pi i} \int_{a-\pi i}^{a+\pi i} \exp(st) F(s) ds, \quad (2.23)$$

which according to Crump [21] can be evaluated using,

$$u(x, t) = \frac{\exp(aT)}{T} \left[\frac{1}{2} F(a) + \sum_{k=1}^{\infty} \operatorname{Re} (F(a + k\pi i/T)) \cos(k\pi i/T) - \operatorname{Im} (F(a + k\pi i/T)) \sin(k\pi i/T) \right]. \quad (2.24)$$

Equation (2.24) is evaluated by assigning $a = \sigma_0 - \ln(E_r)/(2T)$ where $E_r = 10^{-8}$, $\sigma_0 = 0.001$ and $T = 60$ and plotted in Figure 2.3.

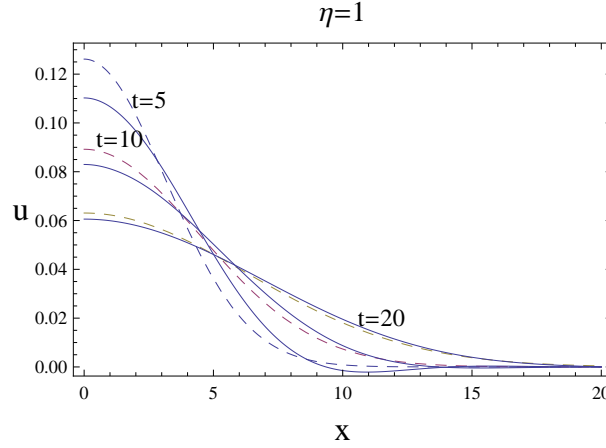


Figure 2.3: Plot comparing the Fourier solution (2.3) (---) and the numerical inversion of the Laplace transform solution of (1.12) (___) for $D = 1$.

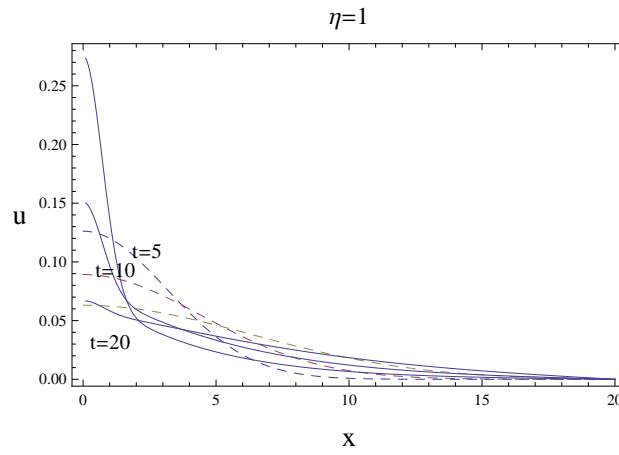


Figure 2.4: Plot comparing the point source solution of the phenomenological equation (2.3) (---) and the numerical inversion of the Laplace transform solution (2.24) (___) with $\nu = 2$ and $\alpha = 10$.

In a similar fashion we apply the same procedure to the two-parameter mixed derivative equation (1.9). A Laplace transform is taken with respect to time, t ,

$$\mathcal{L} \left[\frac{\partial u}{\partial t} - \nu \frac{\partial^2 u}{\partial x^2} - \alpha \frac{\partial^3 u}{\partial t \partial x^2} \right] (s) = 0, \quad (2.25)$$

resulting in the second order differential equation,

$$sF(x) - (s\alpha + \nu)F''(x) - f(x) + \alpha f''(x) = 0. \quad (2.26)$$

The solutions obtained are displayed in Figure 2.4 where the Fourier solution is compared to the point source solution of the phenomenological equation (2.3), with $\nu = 2$ and $\alpha = 10$.

Chapter 3

Stability and Numerical Analyses

It is imperative that we consider the stability of the mixed derivative equation prior to numerical implementation. A stable numerical scheme will give a convergent solution. This is determined using a Von Neumann stability analysis. Warming and Hyett [22] use the modified partial differential equation approach to determine computational stability and a truncated version of the modified equation to gain insight into the dissipative and dispersive errors. The connection between this method and the von-Neumann stability analysis is established. For the purposes of this dissertation, the von-Neumann stability analysis is considered.

3.1 Derivation of the Difference Scheme for the Discrete One-Dimensional Equation

In this section the two-parameter mixed derivative diffusion equation (1.9),

$$\frac{\partial u}{\partial t} - \nu \frac{\partial^2 u}{\partial x^2} - \alpha \frac{\partial^3 u}{\partial t \partial x^2} = 0, \quad (3.1)$$

is investigated for stability using the von Neumann stability analysis according to Momoniat and Harley [5].

Equation (1.9) can be written as,

$$\frac{\partial}{\partial t} \left(u - \alpha \frac{\partial^2 u}{\partial x^2} \right) = \nu \frac{\partial^2 u}{\partial x^2}. \quad (3.2)$$

The right-hand side of the equation is approximated using a central-difference approximation,

$$\frac{\partial^2 u}{\partial x^2} \approx \frac{u_{j+1}^k - 2u_j^k + u_{j-1}^k}{\Delta x^2}, \quad (3.3)$$

for the spatial derivative and for the time derivative, the forward difference,

$$\frac{\partial u}{\partial t} \approx \frac{u_j^{k+1} - u_j^k}{\Delta t}, \quad (3.4)$$

is implemented. The left-hand side of (3.2) is approximated by the implicit Crank-Nicholson approximation [23],

$$\frac{\partial^2 u}{\partial x^2} \approx \frac{u_{j+1}^{k+1} - 2u_j^{k+1} + u_{j-1}^{k+1}}{2\Delta x^2} + \frac{u_{j+1}^k - 2u_j^k + u_{j-1}^k}{2\Delta x^2}, \quad (3.5)$$

which results in the discretised method,

$$\begin{aligned} & (2\alpha + \nu\Delta t)u_{j+1}^{k+1} - 2(2\alpha + \Delta x^2 + \nu\Delta t)u_j^{k+1} + (2\alpha + \nu\Delta t)u_{j-1}^{k+1} \\ & = (2\alpha - \nu\Delta t)u_{j+1}^k - 2(2\alpha + \Delta x^2 - \nu\Delta t)u_j^k + (2\alpha - \nu\Delta t)u_{j-1}^k, \end{aligned} \quad (3.6)$$

where $u_j^k = u(x_j, t_k)$, where $x_j = x_0 + jh$ and $t_k = k\Delta t$ for $j = 0, 1, 2, \dots, n$ and $k = 0, 1, 2, \dots, m$. The number of iterations is m and n is the number of intervals in the domain.

3.2 Von Neumann Stability Analysis

The stability of a numerical scheme depends on the cumulative value of the numerical error at each iteration. If the numerical error at one step causes the numerical error at the next step to increase, the solution diverges and the method is unstable. If the numerical error is constant at all steps then the method is neutrally stable. For a stable method, the numerical error decays out as the iteration progresses.

A von Neumann stability analysis can be performed on a numerical scheme if the continuous PDE of the discretised scheme is linear, if the PDE has constant coefficients with only two independent variables and periodic boundary conditions, and if the method uses a maximum of two time variables. These conditions are met by the case under consideration. By substituting equation (3.7),

$$u_j^k = U^k \exp^{I\omega jh}, \quad I^2 = -1, \quad (3.7)$$

into equation (3.6), where, $h = \Delta x$ and ω is a constant, the result for the amplification factor $g = \frac{U^{k+1}}{U^k}$ is,

$$\frac{U^{k+1}}{U^k} = \frac{(2\alpha - \Delta t\nu)\exp^{I\omega(j+1)h} - 2(2\alpha + \Delta x^2 - \Delta t\nu)\exp^{I\omega jh} + (2\alpha - \Delta t\nu)\exp^{I\omega(j-1)h}}{(2\alpha + \Delta t\nu)\exp^{I\omega(j+1)h} - 2(2\alpha + \Delta x^2 + \Delta t\nu)\exp^{I\omega jh} + (2\alpha - \Delta t\nu)\exp^{I\omega(j-1)h}}. \quad (3.8)$$

Equating the denominators and numerators on the left- and right-hand side of (3.8), we obtain,

$$\begin{aligned} -\frac{1}{2}\exp^{-I\omega jh}U^{k+1} &= (2\alpha - \Delta t\nu) \left(1 - \left(\frac{\exp^{I\omega h} + \exp^{-I\omega h}}{2} \right) \right) + \Delta x^2 \\ &= (2\alpha - \Delta t\nu) (1 - \cos(\omega h)) + \Delta x^2, \end{aligned} \quad (3.9)$$

$$\begin{aligned} -\frac{1}{2}\exp^{-I\omega jh}U^k &= (2\alpha + \Delta t\nu) \left(1 - \left(\frac{\exp^{I\omega h} + \exp^{-I\omega h}}{2} \right) \right) + \Delta x^2 \\ &= (2\alpha + \Delta t\nu) (1 - \cos(\omega h)) + \Delta x^2. \end{aligned} \quad (3.10)$$

Taking the ratio of the resulting equations (3.9) and (3.10), the amplification factor becomes,

$$g = \frac{U^{k+1}}{U^k} = \frac{(2\alpha - \Delta t\nu)(1 - \cos(\omega h)) + \Delta x^2}{(2\alpha + \Delta t\nu)(1 - \cos(\omega h)) + \Delta x^2}. \quad (3.11)$$

Taking the absolute value of g to determine the behaviour of the numerical error we see from,

$$|g| = \left| \frac{(2\alpha - \Delta t\nu)(1 - \cos(\omega h)) + \Delta x^2}{(2\alpha + \Delta t\nu)(1 - \cos(\omega h)) + \Delta x^2} \right|, \quad (3.12)$$

as well as from the basic property of the cosine, $|\cos(\omega h)| \leq 1$ and the triangle inequality, that,

$$|1 - \cos(\omega h)| \leq 2, \quad (3.13)$$

and therefore,

$$|g| = \left| \frac{(2\alpha - \Delta t\nu) + \Delta x^2}{(2\alpha + \Delta t\nu) + \Delta x^2} \right|. \quad (3.14)$$

Hence $|g| < 1$ under certain conditions. The numerical error exhibits a damping property rendering the numerical sequence, (3.6) stable for the case when $\alpha, \nu > 0$.

3.3 Numerical Analysis

In this section, we revisit the discretised equation (3.6), to include boundary conditions. The resulting method is then implemented and its solutions analysed.

We apply the zero-shear boundary conditions,

$$u_{-1}^k = u_1^k, \quad u_{n+1}^k = u_{n-1}^k, \quad (3.15)$$

which are obtained from the central difference approximation,

$$\frac{\partial u}{\partial x} \approx \frac{u_{j+1}^k - u_{j-1}^k}{2\Delta x} \approx 0. \quad (3.16)$$

Let $\eta = 2\alpha$ and $\beta = 2\alpha + \Delta x^2$, then when applying the boundary conditions (3.15) to the numerical scheme, (3.6), we obtain the equations,

$$\begin{aligned} & (\eta + \Delta t\nu)u_{j+1}^{k+1} - 2(\beta + \Delta t\nu)u_j^{k+1} + (\eta + \Delta t\nu)u_{j-1}^{k+1} \\ & = (\eta - \Delta t\nu)u_{j+1}^k - 2(\beta - \Delta t\nu)u_j^k + (\eta - \Delta t\nu)u_{j-1}^k. \end{aligned} \quad (3.17)$$

Equation (3.17), when considering the boundary conditions given by equations (3.15) when $j = 0$ and $j = n$, becomes:

At $j = 0$

$$\begin{aligned} & 2(\eta + \Delta t\nu)u_1^{k+1} - 2(\beta + \Delta t\nu)u_0^{k+1} \\ & = 2(\eta - \Delta t\nu)u_1^k - 2(\beta - \Delta t\nu)u_0^k \end{aligned} \quad (3.18)$$

At $j = n$

$$\begin{aligned} & 2(\eta + \Delta t\nu)u_{n-1}^{k+1} - 2(\beta + \Delta t\nu)u_n^{k+1} \\ & = 2(\eta - \Delta t\nu)u_{n-1}^k - 2(\beta - \Delta t\nu)u_n^k. \end{aligned} \quad (3.19)$$

These equations result in the numerical implementation,

$$AU^{k+1} = BU^k, \quad (3.20)$$

where,

$$A = \begin{bmatrix} -2(\beta + \Delta t\nu) & 2(\eta + \Delta t\nu) & 0 & 0 & \dots & 0 & 0 & 0 & 0 \\ (\eta + \Delta t\nu) & -2(\beta + \Delta t\nu) & (\eta + \Delta t\nu) & 0 & \dots & 0 & 0 & 0 & 0 \\ 0 & (\eta + \Delta t\nu) & -2(\beta + \Delta t\nu) & (\eta + \Delta t\nu) & \dots & 0 & 0 & 0 & 0 \\ \vdots & \vdots & \vdots & \vdots & \ddots & \vdots & \vdots & \vdots & \vdots \\ 0 & 0 & 0 & 0 & \dots & (\eta + \Delta t\nu) & -2(\beta + \Delta t\nu) & (\eta + \Delta t\nu) & 0 \\ 0 & 0 & 0 & 0 & \dots & 0 & (\eta + \Delta t\nu) & -2(\beta + \Delta t\nu) & (\eta + \Delta t\nu) \\ 0 & 0 & 0 & 0 & \dots & 0 & 0 & 2(\eta + \Delta t\nu) & -2(\beta + \Delta t\nu) \end{bmatrix},$$

$$B = \begin{bmatrix} -2(\beta - \Delta t\nu) & 2(\eta - \Delta t\nu) & 0 & 0 & \dots & 0 & 0 & 0 & 0 \\ (\eta - \Delta t\nu) & -2(\beta - \Delta t\nu) & (\eta - \Delta t\nu) & 0 & \dots & 0 & 0 & 0 & 0 \\ 0 & (\eta - \Delta t\nu) & -2(\beta - \Delta t\nu) & (\eta - \Delta t\nu) & \dots & 0 & 0 & 0 & 0 \\ \vdots & \vdots & \vdots & \vdots & \ddots & \vdots & \vdots & \vdots & \vdots \\ 0 & 0 & 0 & 0 & \dots & (\eta - \Delta t\nu) & -2(\beta - \Delta t\nu) & (\eta - \Delta t\nu) & 0 \\ 0 & 0 & 0 & 0 & \dots & 0 & (\eta - \Delta t\nu) & -2(\beta - \Delta t\nu) & (\eta - \Delta t\nu) \\ 0 & 0 & 0 & 0 & \dots & 0 & 0 & 2(\eta - \Delta t\nu) & -2(\beta - \Delta t\nu) \end{bmatrix},$$

$$U^{k+1} = \begin{bmatrix} u_0^{k+1} \\ u_1^{k+1} \\ u_2^{k+1} \\ \vdots \\ u_{n-2}^{k+1} \\ u_{n-1}^{k+1} \\ u_n^{k+1} \end{bmatrix} \quad \text{and} \quad U^k = \begin{bmatrix} u_0^k \\ u_1^k \\ u_2^k \\ \vdots \\ u_{n-2}^k \\ u_{n-1}^k \\ u_n^k \end{bmatrix}.$$

We solve this system above using $n = 200$, $m = 10$, $\Delta t = 0.01$ on the interval $x \in [-5, 5]$.

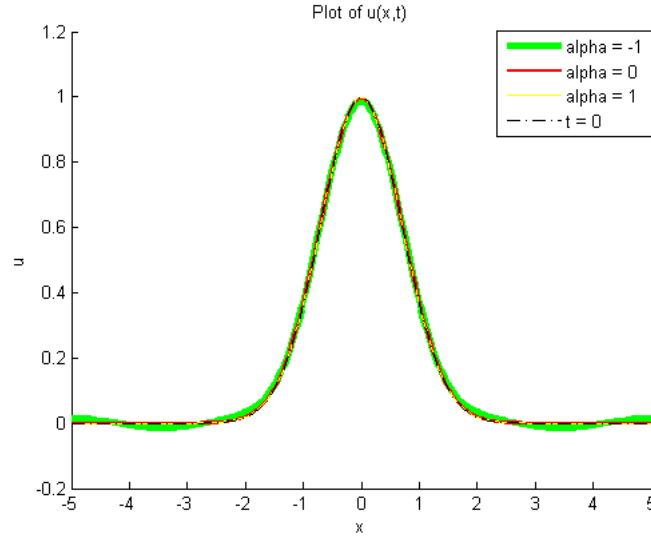


Figure 3.1: Plot of $u(x,t)$ when $\nu = 1$ and $\alpha = -1, 0, 1$.

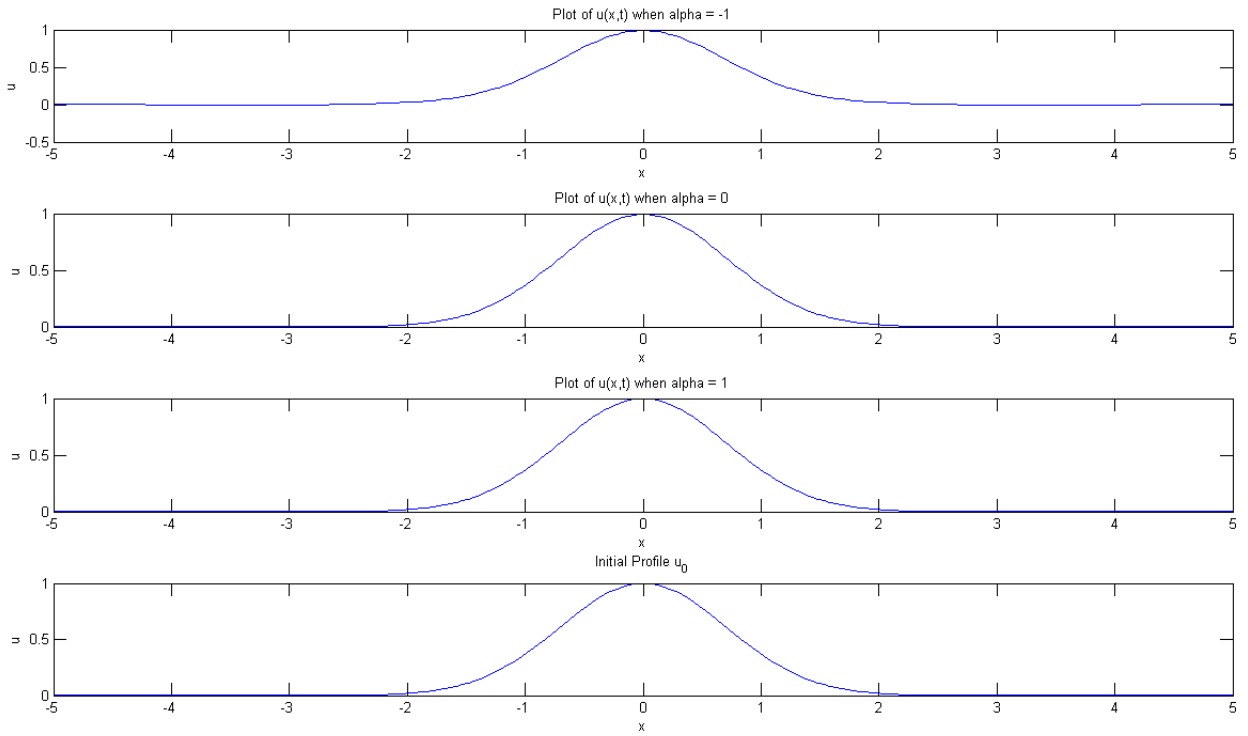


Figure 3.2: Individual plots of $u(x,t)$ when $\nu = 1$ and $\alpha = -1, 0, 1$ and the initial profile.

In Figure 3.1, the oscillation produced by the plot when $\alpha = -1$ and $\nu = 1$ is not as large as is in the article by Momoniat and Harley [5]. However, the oscillation is present for the case when $\alpha = -1$ and $\nu = 1$ in the parabolic mixed derivative diffusion equation, equivalent to the case considered in [5] for $\kappa = -1$.

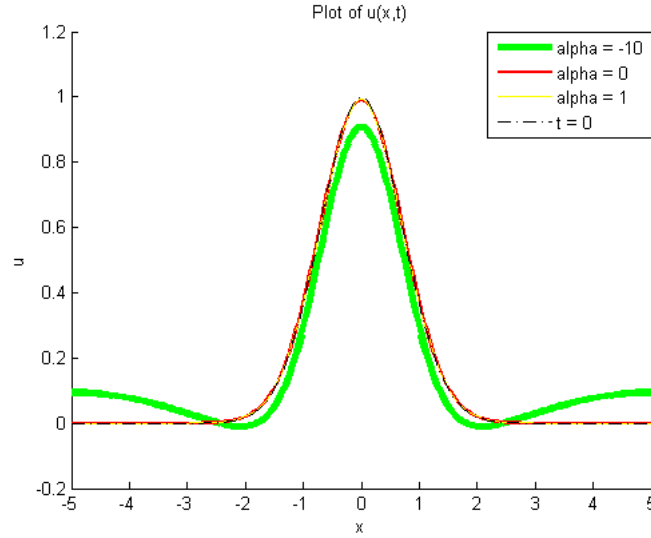


Figure 3.3: Plot of $u(x, t)$ when $\nu = 1$ and $\alpha = -10, 0, 1$.

This can be analytically verified by making the substitution,

$$u(x, t) = U(t) \exp(I\omega x), \quad I^2 = -1, \quad (3.21)$$

where ω is a constant into the parabolic mixed derivative equation, (1.9) to obtain,

$$\frac{\partial U(t)}{\partial t} (1 + \alpha\omega^2) + \nu\omega^2 U(t) = 0. \quad (3.22)$$

Solving this partial differential equation gives the result,

$$U(t) = c_0 \exp\left(-\frac{\nu\omega^2 t}{(1 + \alpha\omega^2)}\right), \quad (3.23)$$

where c_0 is a constant of integration. Substituting (3.23) back into (3.21) gives the final solution,

$$u(x, t) = c_0 \exp\left(-\frac{\nu\omega^2 t}{(1 + \alpha\omega^2)}\right) \exp(I\omega x), \quad I^2 = -1. \quad (3.24)$$

Consider the case when $\nu = 1$, remaining constant for different values of α . From the equation (3.24), it can be seen that for $\alpha \geq 0$, the solution decays to zero at a high rate. For the solutions to decay and not exhibit singularities, for the case when $\alpha < 0$, the condition $\omega^2 < -\frac{1}{\alpha}$ must be met. A very large negative value of α is considered in Figure 3.3. This value is adopted to demonstrate the oscillatory effects for such a value of α . For

the case when $\omega^2 > -\frac{1}{\alpha}$, the oscillations increase greatly as is seen in Figure 3.3, proving the solution itself is not stable under the conditions of $\alpha \ll 0$ and $\nu > 0$ despite the method as a whole being stable. This result is consistent with the von Neumann stability analysis executed in the previous section. In Figure 3.3, we see a decrease in the profile height for $\alpha \ll 0$ while for the other cases of α the profile takes on the closest shape to the initial solution itself.

Chapter 4

Two-Dimensional Diffusion Equation

Momoniat and Harley [5] analyse the two-dimensional analog of the mixed derivative equation and solve it using a Crank-Nicholson method implemented by the Peaceman-Rachford Alternating Direction Implicit scheme [24]. The two-dimensional mixed derivative diffusion equation models the flow of a second grade fluid. In this chapter this approach will be implemented for the two-dimensional analog of the mixed derivative equation (1.9). Thus far the numerical scheme has been shown to be conditionally stable. In the latter part of this chapter the two-dimensional equation implemented using this approach will be shown to be conditionally stable as well.

4.1 Derivation of the Discrete Two-Dimensional Diffusion Equation

We take into consideration the two-dimensional variation of the two-parameter mixed derivative equation (1.9), which is,

$$\frac{\partial u}{\partial t} = \nu \nabla^2 u + \alpha \frac{\partial}{\partial t} \nabla^2 u, \quad (4.1)$$

with,

$$\nabla^2 = \frac{\partial^2}{\partial x^2} + \frac{\partial^2}{\partial y^2}. \quad (4.2)$$

This two-dimensional equation can be expressed as,

$$\frac{\partial u}{\partial t} \left[u - \alpha \left(\frac{\partial^2 u}{\partial x^2} + \frac{\partial^2 u}{\partial y^2} \right) \right] = \nu \left(\frac{\partial^2 u}{\partial x^2} + \frac{\partial^2 u}{\partial y^2} \right). \quad (4.3)$$

This equation is discretised by taking finite-difference approximations on the left-hand side as follows,

$$\frac{\partial^2 u}{\partial x^2} \approx \frac{u_{i+1,j}^k - 2u_{i,j}^k + u_{i-1,j}^k}{\Delta x^2}, \quad (4.4)$$

$$\frac{\partial^2 u}{\partial y^2} \approx \frac{u_{i,j+1}^k - 2u_{i,j}^k + u_{i,j-1}^k}{\Delta y^2}. \quad (4.5)$$

On the right-hand side we implement the Crank-Nicholson Method [23],

$$\frac{\partial^2 u}{\partial x^2} \approx \frac{u_{i+1,j}^{k+1} - 2u_{i,j}^{k+1} + u_{i-1,j}^{k+1}}{\Delta x^2} + \frac{u_{i+1,j}^k - 2u_{i,j}^k + u_{i-1,j}^k}{\Delta x^2}, \quad (4.6)$$

$$\frac{\partial^2 u}{\partial y^2} \approx \frac{u_{i,j+1}^{k+1} - 2u_{i,j}^{k+1} + u_{i,j-1}^{k+1}}{\Delta y^2} + \frac{u_{i,j+1}^k - 2u_{i,j}^k + u_{i,j-1}^k}{\Delta y^2}, \quad (4.7)$$

where $u_{i,j}^k = u(x_i, y_j, t_k)$, $x_i = x_0 + ih$, $y_j = y_0 + jh$, $t_k = k\Delta t$, $i, j = 0, 1, 2, \dots, n$ and $k = 0, 1, 2, \dots, m$.

The time derivative is approximated by the forward difference approximation,

$$\frac{\partial u}{\partial t} \approx \frac{u_{i,j}^{k+1} - u_{i,j}^k}{\Delta t}. \quad (4.8)$$

We substitute (4.4), (4.5), (4.6), and (4.7) into (4.3) to obtain,

$$\begin{aligned} & \rho \frac{\partial u}{\partial t} \left[u - \alpha \left(\frac{u_{i+1,j}^k - 2u_{i,j}^k + u_{i-1,j}^k}{\Delta x^2} + \frac{u_{i,j+1}^k - 2u_{i,j}^k + u_{i,j-1}^k}{\Delta y^2} \right) \right] \\ &= \nu \left(\frac{u_{i+1,j}^{k+1} - 2u_{i,j}^{k+1} + u_{i-1,j}^{k+1} + u_{i+1,j}^k - 2u_{i,j}^k + u_{i-1,j}^k}{\Delta x^2} + \frac{u_{i,j+1}^{k+1} - 2u_{i,j}^{k+1} + u_{i,j-1}^{k+1} + u_{i,j+1}^k - 2u_{i,j}^k + u_{i,j-1}^k}{\Delta y^2} \right). \end{aligned} \quad (4.9)$$

Taking into consideration the time derivative (4.8) on the left-hand side, (4.9) becomes,

$$\begin{aligned}
& u_{i,j}^{k+1} - u_{i,j}^k - \alpha \left(\frac{1}{\Delta x^2} [u_{i+1,j}^{k+1} - 2u_{i,j}^{k+1} + u_{i-1,j}^{k+1} - u_{i+1,j}^k + 2u_{i,j}^k - u_{i-1,j}^k] \right. \\
& \quad \left. + \frac{1}{\Delta y^2} [u_{i,j+1}^{k+1} - 2u_{i,j}^{k+1} + u_{i,j-1}^{k+1} - u_{i,j+1}^k + 2u_{i,j}^k - u_{i,j-1}^k] \right) \\
& = \nu \left(\frac{\Delta t}{2\Delta x^2} [u_{i+1,j}^{k+1} - 2u_{i,j}^{k+1} + u_{i-1,j}^{k+1} + u_{i+1,j}^k - 2u_{i,j}^k + u_{i-1,j}^k] \right. \\
& \quad \left. + \frac{\Delta t}{2\Delta y^2} [u_{i,j+1}^{k+1} - 2u_{i,j}^{k+1} + u_{i,j-1}^{k+1} + u_{i,j+1}^k - 2u_{i,j}^k + u_{i,j-1}^k] \right). \tag{4.10}
\end{aligned}$$

By re-arranging the terms, the resulting discretised equation of (4.1) is the Crank-Nicholson scheme,

$$\begin{aligned}
& u_{i,j}^{k+1} - \left(\frac{\alpha}{\Delta x^2} + \frac{\nu \Delta t}{2\Delta x^2} \right) [u_{i+1,j}^{k+1} - 2u_{i,j}^{k+1} + u_{i-1,j}^{k+1}] \\
& \quad - \left(\frac{\alpha}{\Delta y^2} + \frac{\nu \Delta t}{2\Delta y^2} \right) [u_{i,j+1}^{k+1} - 2u_{i,j}^{k+1} + u_{i,j-1}^{k+1}] \\
& = u_{i,j}^k - \left(\frac{\alpha}{\Delta x^2} - \frac{\nu \Delta t}{2\Delta x^2} \right) [u_{i+1,j}^k - 2u_{i,j}^k + u_{i-1,j}^k] \\
& \quad - \left(\frac{\alpha}{\Delta y^2} - \frac{\nu \Delta t}{2\Delta y^2} \right) [u_{i,j+1}^k - 2u_{i,j}^k + u_{i,j-1}^k]. \tag{4.11}
\end{aligned}$$

4.2 Stability Analysis of the Two-Dimensional Diffusion Equation

Here the stability of the two-dimensional diffusion equation is investigated in a manner similar to what was done previously for the one-dimensional form by substituting,

$$u_{i,j}^k = U^k e^{I\omega_{ij}h^2}, \tag{4.12}$$

into equation (4.11), where $I^2 = -1$, $h = \Delta x$ and ω is a constant. We first investigate,

$$\begin{aligned}
 |u_{i+1,j}^k - 2u_{i,j}^k + u_{i-1,j}^k| &= |U^k e^{I\omega(i+1)jh^2} - 2U^k e^{I\omega ijh^2} + U^k e^{I\omega(i-1)jh^2}| \\
 &= |U^k e^{I\omega ijh^2}| |e^{I\omega jh^2} - 2 + e^{-I\omega jh^2}| \\
 &= 2|U^k e^{I\omega ijh^2}| |\cos(\omega jh^2) - 1| \\
 &\leq 4|U^k e^{I\omega ijh^2}|,
 \end{aligned} \tag{4.13}$$

whose result is as consequence of the fact that $|\cos(\omega jh^2)| \leq 1$ and the triangle inequality.

Similarly,

$$|u_{i+1,j}^k - 2u_{i,j}^k + u_{i-1,j}^k| \leq 4|U^k e^{I\omega ijh^2}|. \tag{4.14}$$

We now substitute (4.12) into (4.11),

$$\begin{aligned}
 &U^{k+1} e^{I\omega ijh^2} - \left(\frac{\alpha}{\Delta x^2} + \frac{\nu \Delta t}{2\Delta x^2} \right) \left[(U^{k+1} e^{I\omega ijh^2})(e^{I\omega jh^2} - 2 + e^{-I\omega jh^2}) \right] \\
 &\quad - \left(\frac{\alpha}{\Delta y^2} + \frac{\nu \Delta t}{2\Delta y^2} \right) \left[(U^{k+1} e^{I\omega ijh^2})(e^{I\omega ih^2} - 2 + e^{-I\omega ih^2}) \right] \\
 &= U^k e^{I\omega ijh^2} - \left(\frac{\alpha}{\Delta x^2} - \frac{\nu \Delta t}{2\Delta x^2} \right) \left[(U^k e^{I\omega ijh^2})(e^{I\omega jh^2} - 2 + e^{-I\omega jh^2}) \right] \\
 &\quad - \left(\frac{\alpha}{\Delta y^2} - \frac{\nu \Delta t}{2\Delta y^2} \right) \left[(U^k e^{I\omega ijh^2})(e^{I\omega ih^2} - 2 + e^{-I\omega ih^2}) \right],
 \end{aligned} \tag{4.15}$$

and using (4.13) and (4.14) $|g| = \left| \frac{U^{k+1}}{U^k} \right|$ becomes,

$$|g| = \left| \frac{1 - \left(\frac{\alpha}{\Delta x^2} - \frac{\nu \Delta t}{2\Delta x^2} \right) [(U^k e^{I\omega ijh^2})(e^{I\omega jh^2} - 2 + e^{-I\omega jh^2})] - \left(\frac{\alpha}{\Delta y^2} - \frac{\nu \Delta t}{2\Delta y^2} \right) [(U^k e^{I\omega ijh^2})(e^{I\omega ih^2} - 2 + e^{-I\omega ih^2})]}{1 - \left(\frac{\alpha}{\Delta x^2} + \frac{\nu \Delta t}{2\Delta x^2} \right) [(U^{k+1} e^{I\omega ijh^2})(e^{I\omega jh^2} - 2 + e^{-I\omega jh^2})] - \left(\frac{\alpha}{\Delta y^2} + \frac{\nu \Delta t}{2\Delta y^2} \right) [(U^{k+1} e^{I\omega ijh^2})(e^{I\omega ih^2} - 2 + e^{-I\omega ih^2})]} \right|, \tag{4.16}$$

which simplifies to,

$$|g| = \left| \frac{U^{k+1}}{U^k} \right| \leq \left| \frac{1 - 4\left(\frac{\alpha}{\Delta x^2} - \frac{\nu \Delta t}{2\Delta x^2} \right) - 4\left(\frac{\alpha}{\Delta y^2} - \frac{\nu \Delta t}{2\Delta y^2} \right)}{1 - 4\left(\frac{\alpha}{\Delta x^2} + \frac{\nu \Delta t}{2\Delta x^2} \right) - 4\left(\frac{\alpha}{\Delta y^2} + \frac{\nu \Delta t}{2\Delta y^2} \right)} \right|. \tag{4.17}$$

When $\alpha < 0$ and $\nu > 0$, $|g| \geq 1$ and the solution diverges whereas when $\alpha, \nu > 0$, $|g| < 1$. Therefore the discretised two-dimensional diffusion equation (4.11) is conditionally stable for the case when $\alpha, \nu > 0$.

4.3 Peaceman-Rachford ADI Scheme with Crank-Nicholson Implementation: Numerical Analysis and Results

4.3.1 Accuracy of Scheme

Here we consider second-order central difference approximations for the spatial derivatives and the Crank-Nicholson approximation to second-order spatial derivatives in matrix form,

$$\frac{\partial^2 u}{\partial x^2} \approx Au^k, \quad \frac{\partial^2 u}{\partial y^2} \approx Bu^k, \quad (4.18)$$

where,

$$(Au^k)_{i,j} = \frac{1}{\Delta x^2} [u_{i+1,j}^k - 2u_{i,j}^k + u_{i-1,j}^k], \quad (4.19)$$

$$(Bu^k)_{i,j} = \frac{1}{\Delta y^2} [u_{i,j+1}^k - 2u_{i,j}^k + u_{i,j-1}^k]. \quad (4.20)$$

The Crank-Nicholson approximation is as follows,

$$\frac{\partial^2 u}{\partial x^2} \approx \frac{1}{2}Au^{k+1} + \frac{1}{2}Au^k, \quad (4.21)$$

$$\frac{\partial^2 u}{\partial y^2} \approx \frac{1}{2}Bu^{k+1} + \frac{1}{2}Bu^k. \quad (4.22)$$

The time derivative is approximated by,

$$\frac{\partial u}{\partial t} \approx \frac{u^{k+1} - u^k}{\Delta t}. \quad (4.23)$$

Substituting (4.20), (4.22) and (4.23) into (4.3) we have,

$$\frac{\partial}{\partial t} [u - \alpha(Au^k + Bu^k)] = \nu \left(\frac{1}{2}(A+B)u^{k+1} + \frac{1}{2}(A+B)u^k \right), \quad (4.24)$$

$$\left[\frac{u^{k+1} - u^k}{\Delta t} \right] - \alpha(A+B) \left[\frac{u^{k+1} - u^k}{\Delta t} \right] = \nu \left(\frac{1}{2}(A+B)u^{k+1} + \frac{1}{2}(A+B)u^k \right), \quad (4.25)$$

which upon regrouping gives,

$$\left[I - \left(\alpha + \frac{\nu \Delta t}{2} \right) (A + B) \right] u^{k+1} = \left[I - \left(\alpha - \frac{\nu \Delta t}{2} \right) (A + B) \right] u^k. \quad (4.26)$$

This can be re-written as,

$$u^{k+1} = u^k + \left(\alpha + \frac{\nu \Delta t}{2} \right) (A + B) u^{k+1} - \left(\alpha - \frac{\nu \Delta t}{2} \right) (A + B) u^k. \quad (4.27)$$

If we now take a half-step implicitly in the direction of A and explicitly in the direction of B we obtain,

$$u^{k+\frac{1}{2}} = u^k + \left(\alpha + \frac{\nu \Delta t}{2} \right) A u^{k+\frac{1}{2}} - \left(\alpha - \frac{\nu \Delta t}{2} \right) B u^k, \quad (4.28)$$

and taking another half-step implicitly in the direction of B and explicitly in the direction of A,

$$u^{k+1} = u^{k+\frac{1}{2}} + \left(\alpha + \frac{\nu \Delta t}{2} \right) B u^{k+1} - \left(\alpha - \frac{\nu \Delta t}{2} \right) A u^{k+\frac{1}{2}}. \quad (4.29)$$

Therefore (4.28) and (4.29) can be written in two stages:

STAGE 1:

$$\left[I - \left(\alpha + \frac{\nu \Delta t}{2} \right) A \right] u^{k+\frac{1}{2}} = \left[I - \left(\alpha - \frac{\nu \Delta t}{2} \right) B \right] u^k, \quad (4.30)$$

STAGE 2:

$$\left[I - \left(\alpha + \frac{\nu \Delta t}{2} \right) B \right] u^{k+1} = \left[I - \left(\alpha - \frac{\nu \Delta t}{2} \right) A \right] u^{k+\frac{1}{2}}. \quad (4.31)$$

Stability can easily be shown by multiplying out STAGE 1 and STAGE 2 and dividing through by $u^{k+\frac{1}{2}}$,

$$\left[I - \left(\alpha + \frac{\nu \Delta t}{2} \right) A \right] \left[I - \left(\alpha + \frac{\nu \Delta t}{2} \right) B \right] u^{k+1} = \left[I - \left(\alpha - \frac{\nu \Delta t}{2} \right) A \right] \left[I - \left(\alpha - \frac{\nu \Delta t}{2} \right) B \right] u^k. \quad (4.32)$$

Multiplying out (4.32) we get,

$$\left[I - \left(\alpha + \frac{\nu \Delta t}{2} \right) (A + B) \right] u^{k+1} = \left[I - \left(\alpha - \frac{\nu \Delta t}{2} \right) (A + B) \right] u^k + O(\Delta t)^2. \quad (4.33)$$

Therefore the Peaceman-Rachford ADI method has the stability of the Crank-Nicholson method accurate to $O(\Delta t)^2$.

4.3.2 Numerical Results

STAGE 1:

Using (4.19) we can write (4.30) as,

$$u_{i,j}^{k+\frac{1}{2}} - \left(\frac{\alpha}{\Delta x^2} + \frac{\nu \Delta t}{2\Delta x^2} \right) [u_{i+1,j}^{k+\frac{1}{2}} - 2u_{i,j}^{k+\frac{1}{2}} + u_{i-1,j}^{k+\frac{1}{2}}] = u_{i,j}^k - \left(\frac{\alpha}{\Delta y^2} - \frac{\nu \Delta t}{2\Delta y^2} \right) [u_{i,j+1}^k - 2u_{i,j}^k + u_{i,j-1}^k]. \quad (4.34)$$

Let,

$$s_x^A = \left(\frac{\alpha}{\Delta x^2} + \frac{\nu \Delta t}{2\Delta x^2} \right), \quad s_y^B = \left(\frac{\alpha}{\Delta y^2} - \frac{\nu \Delta t}{2\Delta y^2} \right). \quad (4.35)$$

Substituting (4.35) into (4.34) we obtain,

$$(1 + 2s_x^A)u_{i,j}^{k+\frac{1}{2}} - s_x^A u_{i+1,j}^{k+\frac{1}{2}} - s_x^A u_{i-1,j}^{k+\frac{1}{2}} = (1 + 2s_y^B)u_{i,j}^k - s_y^B u_{i,j+1}^k - s_y^B u_{i,j-1}^k. \quad (4.36)$$

In stage 1, the x index varies on the left-hand side implicitly in the x-direction only, with a fixed y index. We find $u_{i,j}^{k+\frac{1}{2}}(:, j)$ by solving the tri-diagonal system (boundary conditions have not yet been considered) as follows,

$$Au_{i,j}^{k+\frac{1}{2}}(:, j) = b(i), \quad (4.37)$$

where,

$$A = \begin{bmatrix} 1 + 2s_x^A & -s_x^A & 0 & \dots & 0 & 0 & 0 \\ -s_x^A & 1 + 2s_x^A & -s_x^A & \dots & 0 & 0 & 0 \\ \vdots & \vdots & \vdots & \ddots & \vdots & \vdots & \vdots \\ 0 & 0 & 0 & \dots & -s_x^A & 1 + 2s_x^A & -s_x^A \\ 0 & 0 & 0 & \dots & 0 & -s_x^A & 1 + 2s_x^A \end{bmatrix},$$

$$b(i) = (1 + 2s_y^B)u_{i,j}^k - s_y^B u_{i,j+1}^k - s_y^B u_{i,j-1}^k. \quad (4.38)$$

We consider the central differences approximation to the spatial derivatives,

$$\frac{\partial u}{\partial x} \approx \frac{u_{i+1,j}^k - u_{i-1,j}^k}{2\Delta x}, \quad \frac{\partial u}{\partial y} \approx \frac{u_{i,j+1}^k - u_{i,j-1}^k}{2\Delta y}, \quad (4.39)$$

and apply the zero-shear boundary conditions $\frac{\partial u}{\partial x} \approx 0$, $\frac{\partial u}{\partial y} \approx 0$ to obtain,

$$u_{1,j}^k = u_{-1,j}^k, \quad u_{n+1,j}^k = u_{n-1,j}^k, \quad u_{i,1}^k = u_{i,-1}^k, \quad u_{i,n+1}^k = u_{i,n-1}^k. \quad (4.40)$$

Stage 1 of the method is implemented numerically using the following system of equations,

$$\begin{bmatrix} 1 + 2s_x^A & -2s_x^A & 0 & \dots & 0 & 0 & 0 \\ -s_x^A & 1 + 2s_x^A & -s_x^A & \dots & 0 & 0 & 0 \\ \vdots & \vdots & \vdots & \ddots & \vdots & \vdots & \vdots \\ 0 & 0 & 0 & \dots & -s_x^A & 1 + 2s_x^A & -s_x^A \\ 0 & 0 & 0 & \dots & 0 & -2s_x^A & 1 + 2s_x^A \end{bmatrix} \begin{bmatrix} u_{0,j}^{k+\frac{1}{2}} \\ u_{1,j}^{k+\frac{1}{2}} \\ \vdots \\ u_{n-1,j}^{k+\frac{1}{2}} \\ u_{n,j}^{k+\frac{1}{2}} \end{bmatrix} \quad (4.41)$$

$$= \begin{bmatrix} (1 + 2s_y^B)u_{0,j}^k - s_y^B u_{0,j+1}^k - s_y^B u_{0,j-1}^k \\ (1 + 2s_y^B)u_{1,j}^k - s_y^B u_{1,j+1}^k - s_y^B u_{1,j-1}^k \\ \vdots \\ (1 + 2s_y^B)u_{n-1,j}^k - s_y^B u_{n-1,j+1}^k - s_y^B u_{n-1,j-1}^k \\ (1 + 2s_y^B)u_{n,j}^k - s_y^B u_{n,j+1}^k - s_y^B u_{n,j-1}^k \end{bmatrix}. \quad (4.42)$$

STAGE 2:

We can write equation (4.31) as,

$$u_{i,j}^{k+1} - \left(\frac{\alpha}{\Delta y^2} + \frac{\nu \Delta t}{2\Delta y^2} \right) [u_{i,j+1}^{k+1} - 2u_{i,j}^{k+1} + u_{i,j-1}^{k+1}] = u_{i,j}^{k+\frac{1}{2}} - \left(\frac{\alpha}{\Delta x^2} - \frac{\nu \Delta t}{2\Delta x^2} \right) [u_{i+1,j}^{k+\frac{1}{2}} - 2u_{i,j}^{k+\frac{1}{2}} + u_{i-1,j}^{k+\frac{1}{2}}]. \quad (4.43)$$

Let,

$$s_y^A = \left(\frac{\alpha}{\Delta y^2} + \frac{\nu \Delta t}{2\Delta y^2} \right), \quad s_x^B = \left(\frac{\alpha}{\Delta x^2} - \frac{\nu \Delta t}{2\Delta x^2} \right). \quad (4.44)$$

Substituting (4.44) into (4.43) gives,

$$(1 + 2s_y^A)u_{i,j}^{k+1} - s_y^A u_{i,j+1}^{k+1} - s_y^A u_{i,j-1}^{k+1} = (1 + 2s_x^B)u_{i,j}^{k+\frac{1}{2}} - s_x^B u_{i+1,j}^{k+\frac{1}{2}} - s_x^B u_{i-1,j}^{k+\frac{1}{2}}. \quad (4.45)$$

In stage 2, the y index varies on the left-hand side implicitly in the y-direction only, with a fixed x index. We find $u_{i,j}^{k+1}(i, :)$ by solving the tri-diagonal system (boundary conditions have not yet been considered) as follows,

$$Au_{i,j}^{k+1}(i, :) = b(j), \quad (4.46)$$

where,

$$A = \begin{bmatrix} 1 + 2s_y^A & -s_y^A & 0 & \dots & 0 & 0 & 0 \\ -s_y^A & 1 + 2s_y^A & -s_y^A & \dots & 0 & 0 & 0 \\ \vdots & \vdots & \vdots & \ddots & \vdots & \vdots & \vdots \\ 0 & 0 & 0 & \dots & -s_y^A & 1 + 2s_y^A & -s_y^A \\ 0 & 0 & 0 & \dots & 0 & -s_y^A & 1 + 2s_y^A \end{bmatrix},$$

$$b(j) = (1 + 2s_x^B)u_{i,j}^{k+\frac{1}{2}} - s_x^B u_{i+1,j}^{k+\frac{1}{2}} - s_x^B u_{i-1,j}^{k+\frac{1}{2}}, \quad (4.47)$$

Similarly to stage 1, we consider the zero shear boundary conditions, (4.40), and numerically implement the method using the following system of equations for stage 2,

$$\begin{bmatrix} 1 + 2s_y^A & -2s_y^A & 0 & \dots & 0 & 0 & 0 \\ -s_y^A & 1 + 2s_y^A & -s_y^A & \dots & 0 & 0 & 0 \\ \vdots & \vdots & \vdots & \ddots & \vdots & \vdots & \vdots \\ 0 & 0 & 0 & \dots & -s_y^A & 1 + 2s_y^A & -s_y^A \\ 0 & 0 & 0 & \dots & 0 & -2s_y^A & 1 + 2s_y^A \end{bmatrix} \begin{bmatrix} u_{i,0}^{k+1} \\ u_{i,1}^{k+1} \\ \vdots \\ u_{i,n-1}^{k+1} \\ u_{i,n}^{k+1} \end{bmatrix} \quad (4.48)$$

$$= \begin{bmatrix} (1 + 2s_x^B)u_{i,0}^{k+\frac{1}{2}} - s_x^B u_{i+1,0}^{k+\frac{1}{2}} - s_x^B u_{i-1,0}^{k+\frac{1}{2}} \\ (1 + 2s_x^B)u_{i,1}^{k+\frac{1}{2}} - s_x^B u_{i+1,1}^{k+\frac{1}{2}} - s_x^B u_{i-1,1}^{k+\frac{1}{2}} \\ \vdots \\ (1 + 2s_x^B)u_{i,n-1}^{k+\frac{1}{2}} - s_x^B u_{i+1,n-1}^{k+\frac{1}{2}} - s_x^B u_{i-1,n-1}^{k+\frac{1}{2}} \\ (1 + 2s_x^B)u_{i,n}^{k+\frac{1}{2}} - s_x^B u_{i+1,n}^{k+\frac{1}{2}} - s_x^B u_{i-1,n}^{k+\frac{1}{2}} \end{bmatrix}. \quad (4.49)$$

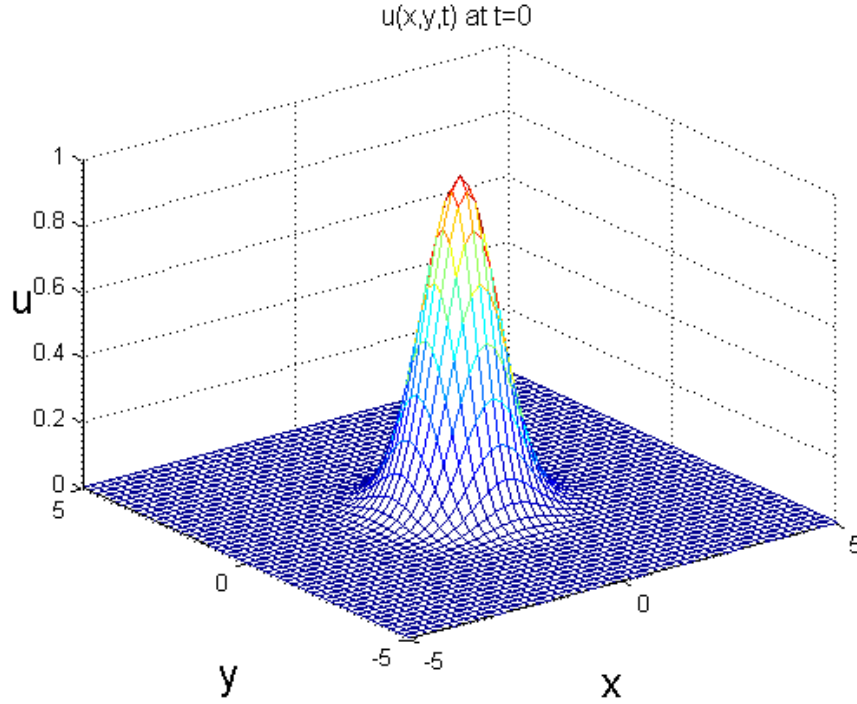


Figure 4.1: Plot of the Initial Profile $u(x, y, t) = e^{(x^2 - y^2)}$ at $t=0$.

In order to implement the method, we choose $\Delta t = 0.1$, $\Delta x = \Delta y = \frac{(b-a)}{(n)}$ where $a = -5$, $b = 5$ and $n = 50$. The Figure 4.1 above represents the initial curve, that is,

$$u(x, y, 0) = u^0(x_i, y_j) = \exp(-x_i^2 - y_j^2). \quad (4.50)$$

The results in Figure 4.2 are in correspondence with the solutions produced in [5] for $\kappa = 0$ and $\kappa = 1$ respectively. When $\alpha = 0$ and $\nu = 1$ there is a decrease in the profile height in comparison to the initial solution. At $\alpha = 1$ and $\nu = 1$, the decrease in the profile height in comparison to the initial curve is at a slower rate than when $\alpha = 0$ and $\nu = 1$. A more in-depth discussion of the meaning behind the results obtained will follow in the next section.

4.4 Physical Interpretation of Results

In this section the behaviour of the results is demonstrated according to the physical significance of the parameters, described in the introductory section. Here we examine the relationship between the viscous and inertia effects as seen from the numerical results produced for equation (1.9).

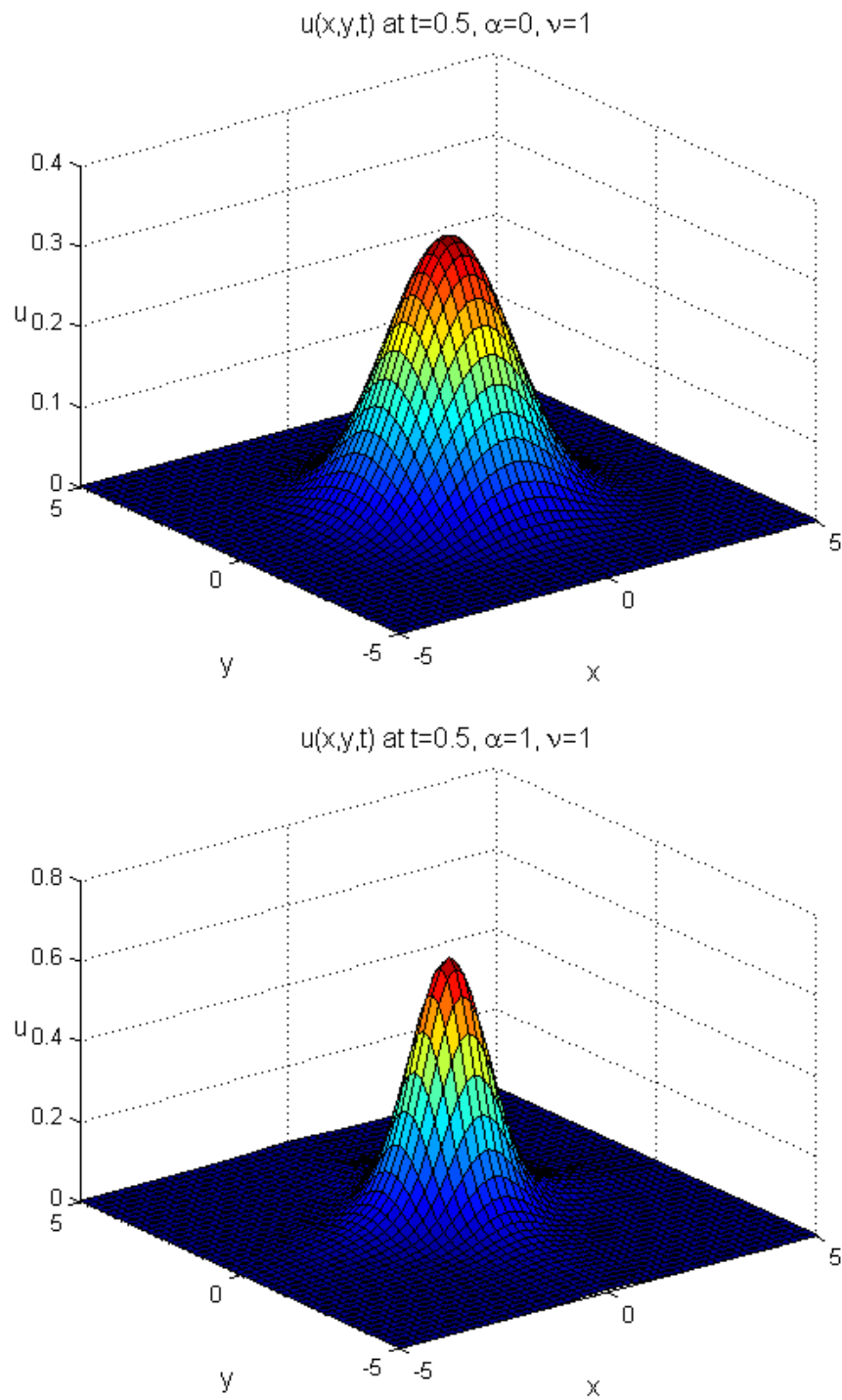


Figure 4.2: Plot of $u(x,y,t)$ for $\alpha = 0$ and $\nu = 1$ (top) and for $\alpha = 1$ and $\nu = 1$ (bottom).

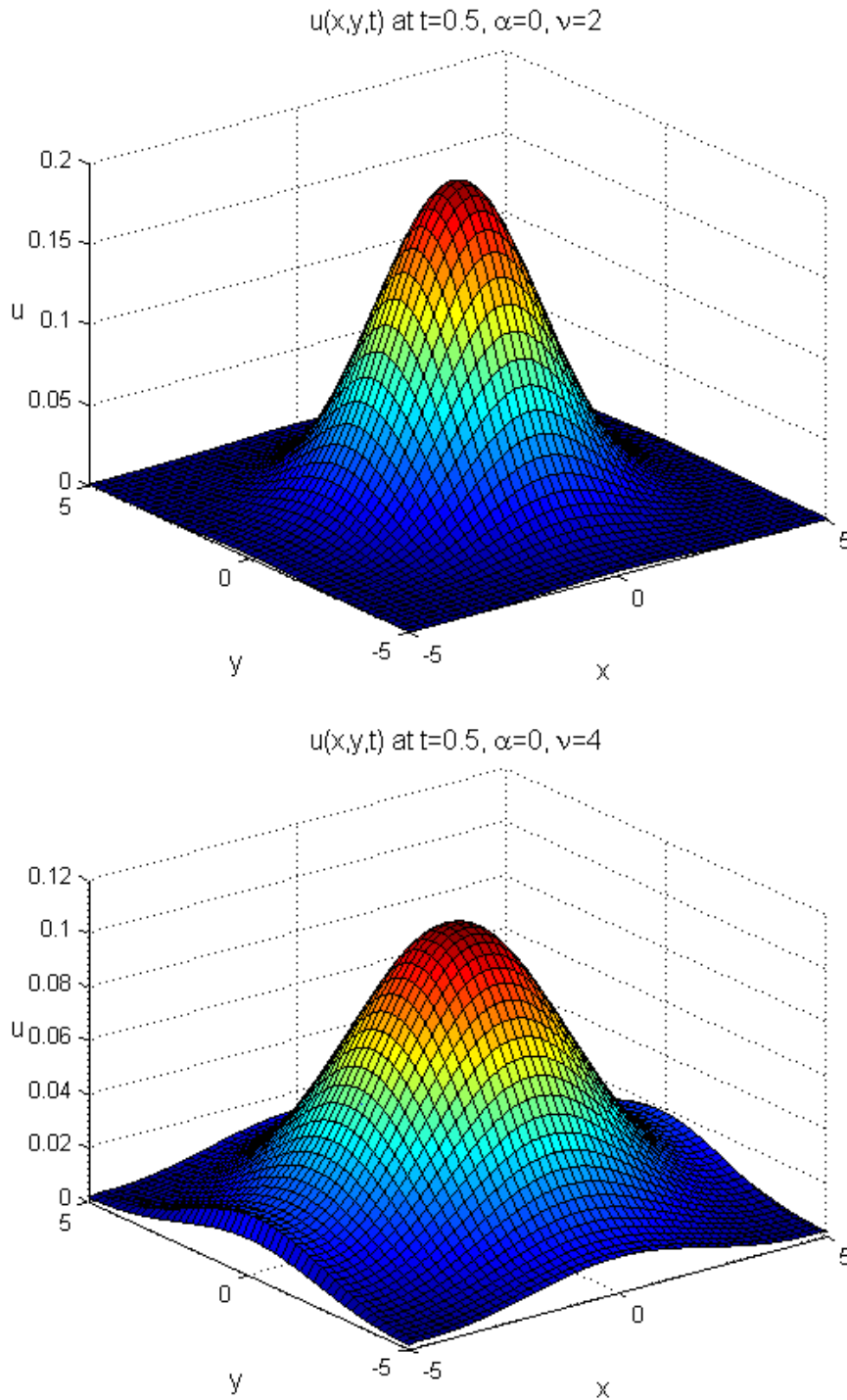


Figure 4.3: Plot of $u(x,y,t)$ displaying diffusion effects for $\alpha = 0$ and $\nu = 2$ (top) and for $\alpha = 0$ and $\nu = 4$ (bottom).

It must be noted that the parameter values chosen for α and ν are to demonstrate the resulting numerical effects.

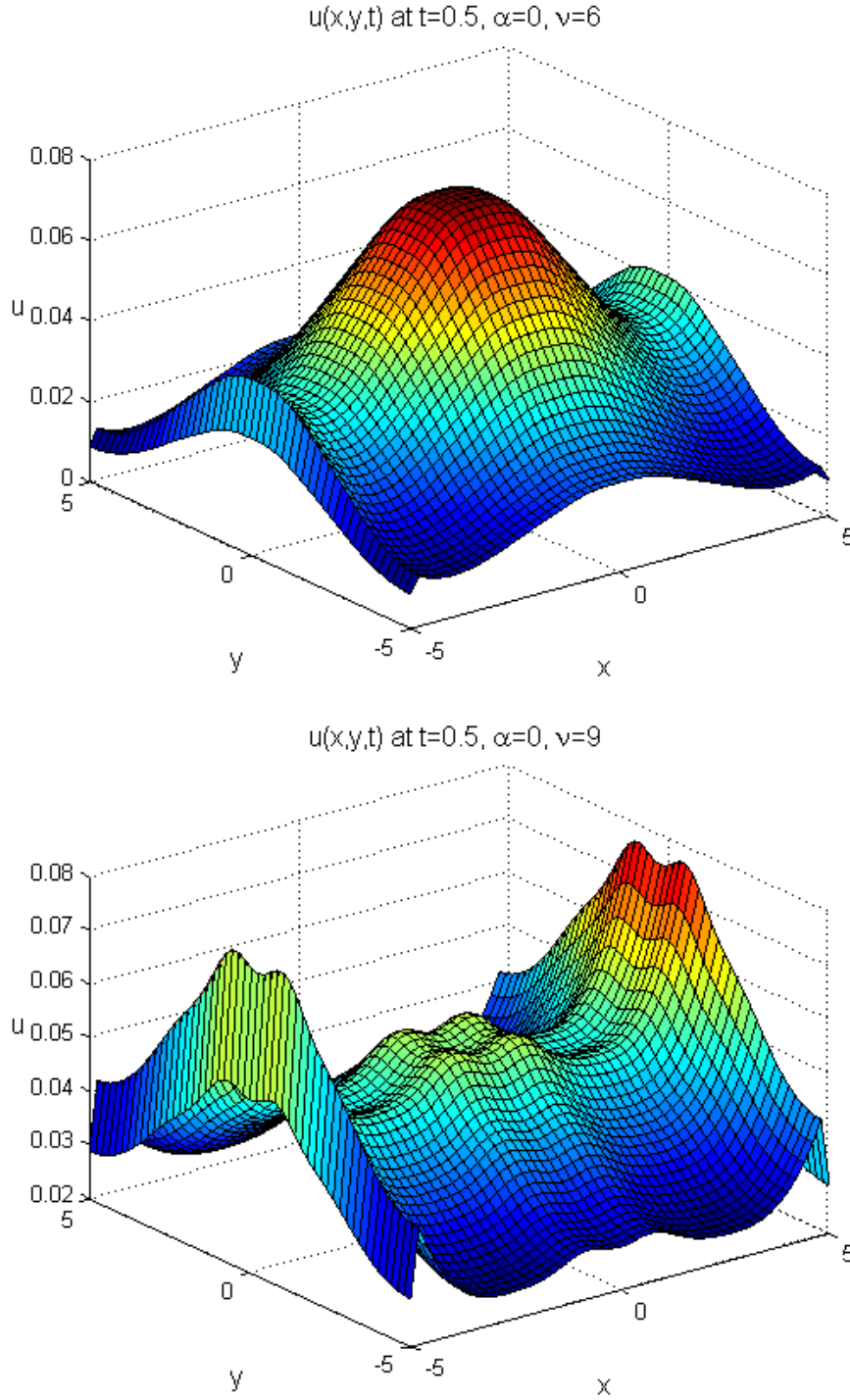


Figure 4.4: Plot of $u(x, y, t)$ displaying diffusion effects for $\alpha = 0$ and $\nu = 6$ (top) and for $\alpha = 0$ and $\nu = 9$ (bottom).

In the Figure 4.3 and Figure 4.4, the value of α is kept constant at 0 to show the sole effects of diffusion, by varying the value of ν . As the values of ν increase, the profile exhibits a dispersion effect, a broadening of the profile, while the profile height decreases due to the zero effects of the viscoelasticity. As discussed in chapter 1, it is evident that as ν is increased, the Reynolds number is smaller than 1, $Re \ll 1$, given that the effects of inertia,

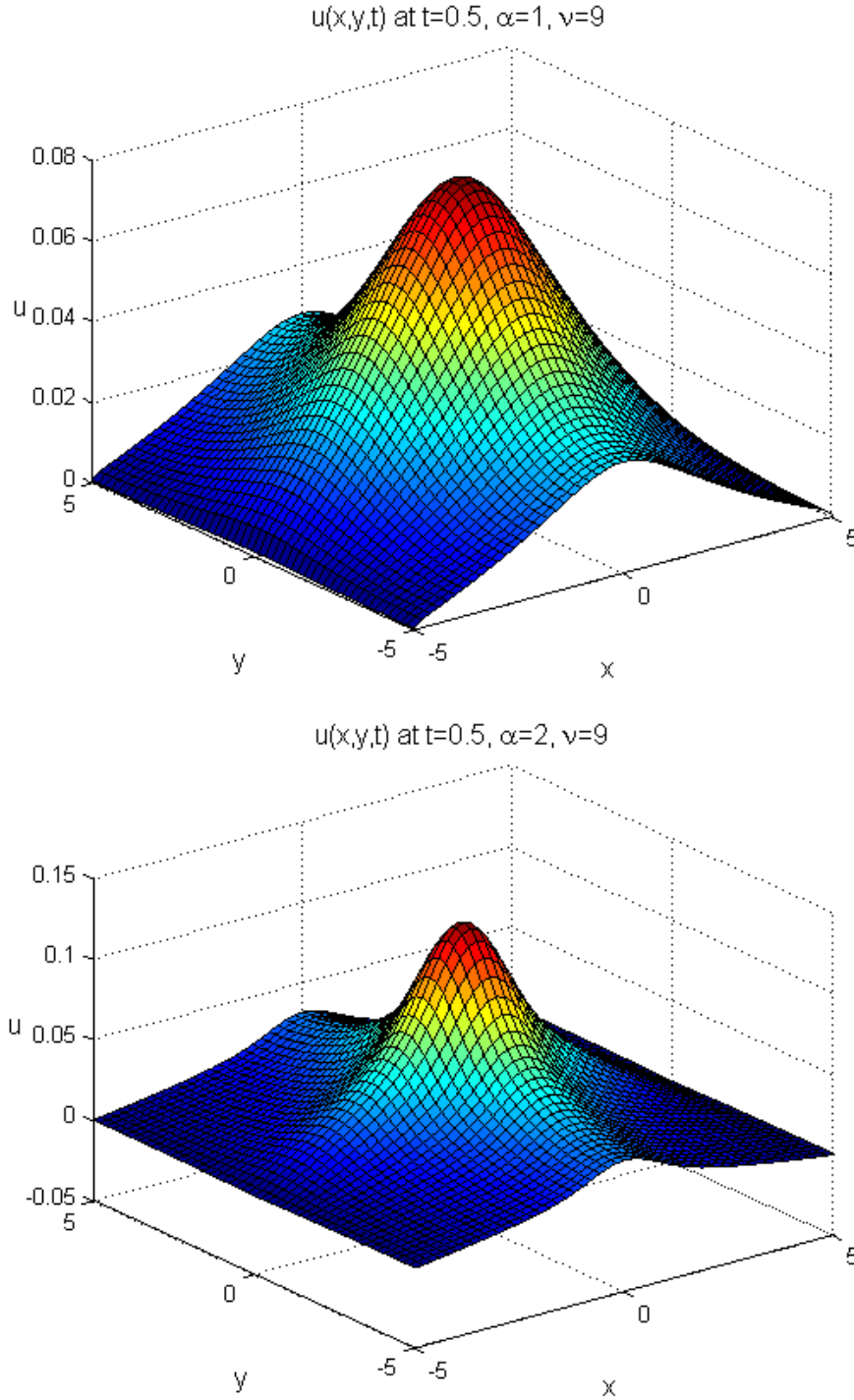


Figure 4.5: Plot of $u(x,y,t)$ displaying viscoelastic effects for $\alpha = 1$ and $\nu = 9$ (top) and for $\alpha = 2$ and $\nu = 9$ (bottom).

UL , is much smaller than ν . Such a fluid exhibits slow viscous flow. Introducing the viscoelastic effects by setting $\alpha = 1$, as in Figure 4.5 we see that the very oscillatory profile, when $\alpha = 0$ becomes more stable displaying an increase and sharpening of the profile height. The increase in the profile height caused by varying the constant α stabilises the volatility

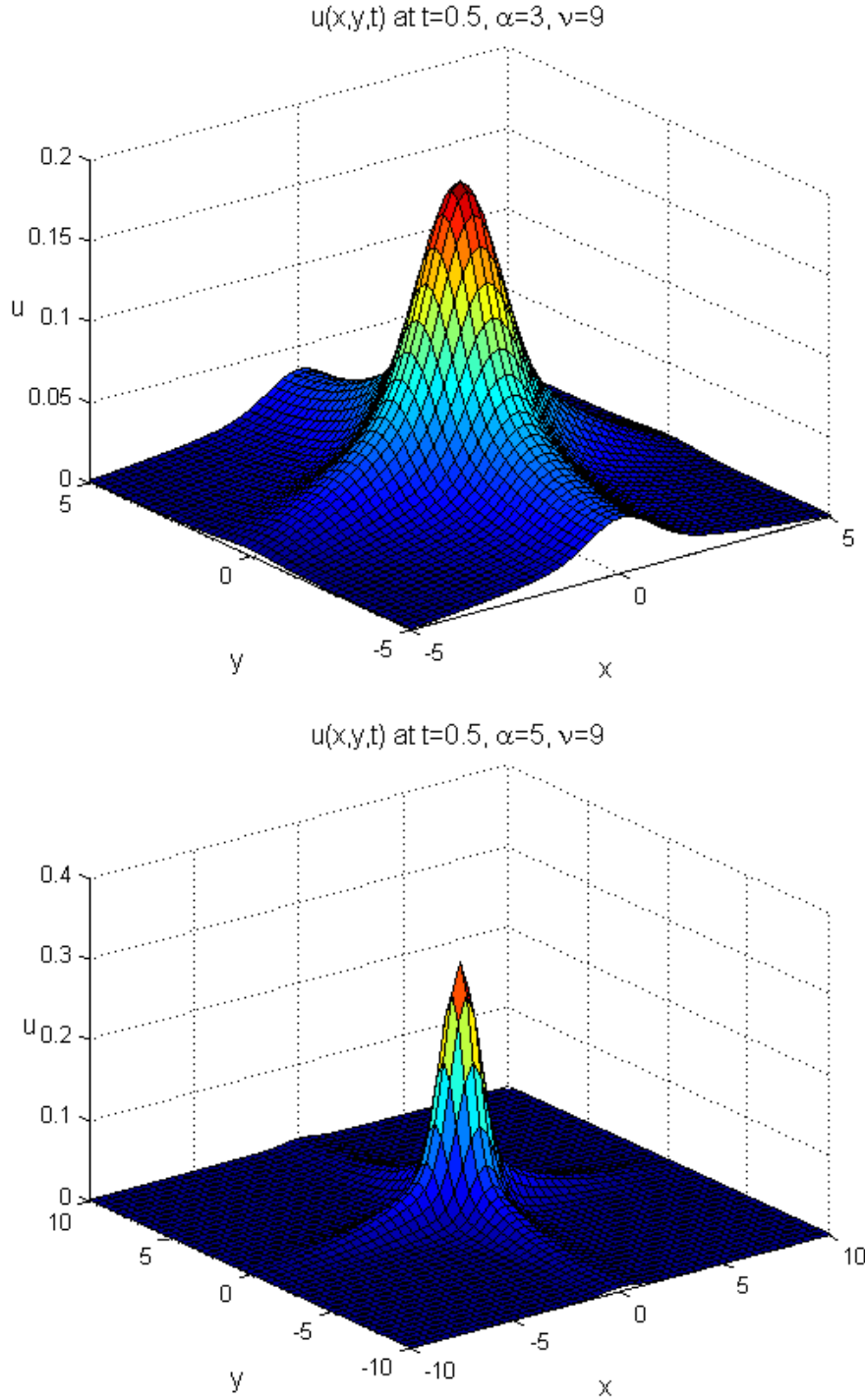


Figure 4.6: Plot of $u(x,y,t)$ displaying viscoelastic effects for $\alpha = 3$ and $\nu = 9$ (top) and for $\alpha = 5$ and $\nu = 9$ (bottom) .

caused by the diffusion effects in the solution, as in Figure 4.5 and Figure 4.6.

Keeping ν constant at 9, while changing α we can see the profile exhibiting changes in sharpness and height as in Figure 4.6. At such a high viscosity, the presence of α is imperative in order to have a realistic viscoelastic fluid solution. As α is increased, for

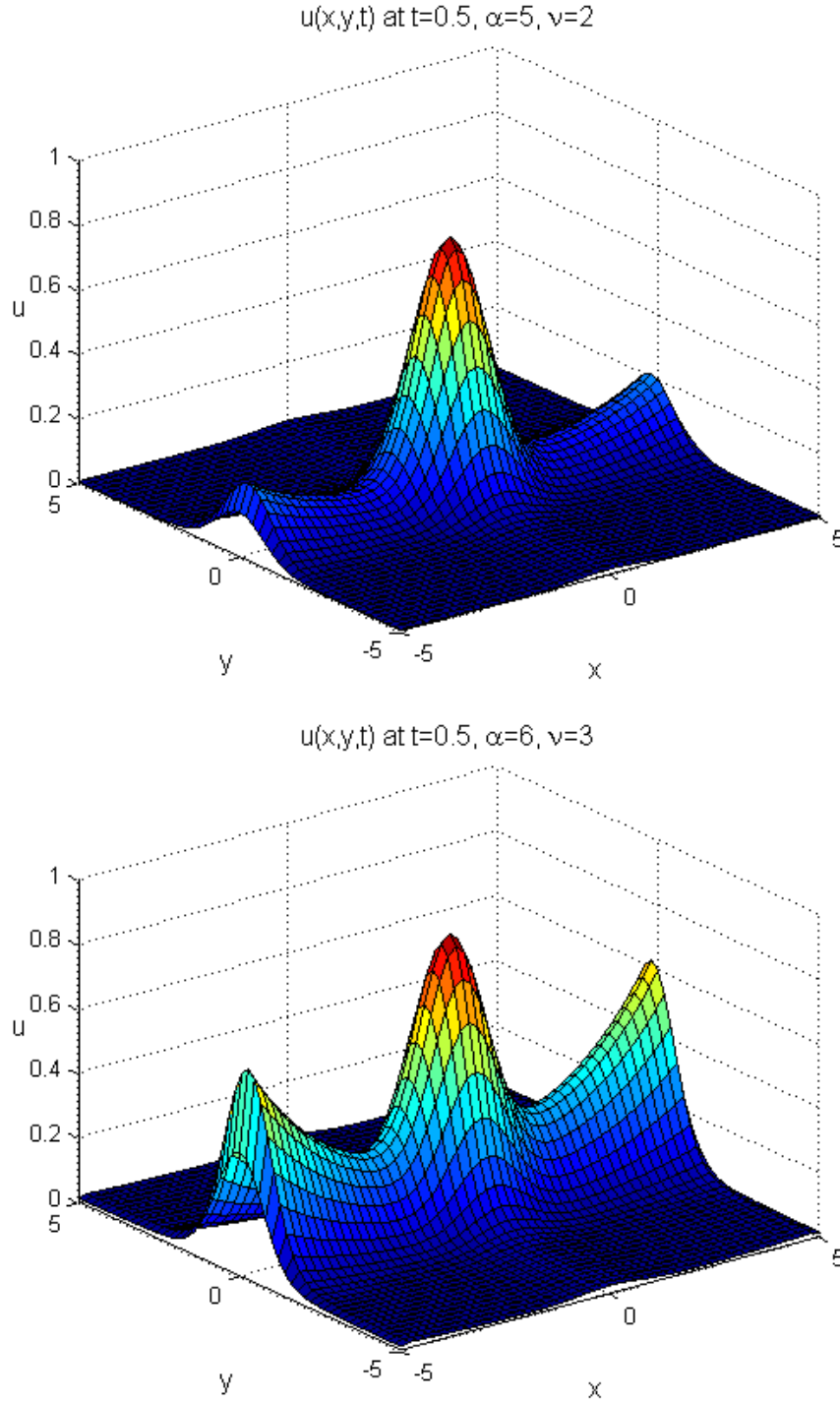


Figure 4.7: Plot of $u(x, y, t)$ for $\alpha = 5$ and $\nu = 2$ (top) and for $\alpha = 6$ and $\nu = 3$ (bottom) .

a constant value of ν , the solution exhibits dominant viscoelastic effects. That is, $\frac{L^2}{\alpha} \ll Re = \frac{UL}{\nu}$. Expanding the range to $y \in [-10, 10]$ and the domain to $x \in [-10, 10]$ leads to results which show some lifting along the boundaries as in the bottom plot of Figure 4.6 for $\alpha = 5$ and $\nu = 9$. This is just a mathematical effect of the boundary conditions, $\frac{\partial u}{\partial x} \approx 0$ and $\frac{\partial u}{\partial y} \approx 0$. Increasing α to values greater than that of ν as in Figure 4.7, we see for the first plot, when $\alpha = 5$ and $\nu = 2$ that there is major lifting in the boundaries. The

solution exhibits very odd behaviour for values of $\alpha > \nu$, that is, the ratio, $D = \frac{\nu}{\alpha} < 1$. The solution for this case, becomes unpredictable and diverges totally from the profile of the initial solution when $\alpha > \nu$ for high values of both α and ν . This is, however, improved drastically by introducing a sixth order accurate high-order compact ADI method, as will be discussed in the next chapter.

Chapter 5

High-Order Compact ADI Method

In this section we investigate a high-order compact ADI method as in the paper by Chen and Liu [25] for the two-dimensional equation analysed in the previous chapter. The high-order ADI as opposed to the Peaceman-Rachford ADI method provides a higher accuracy. As before, we employ a finite difference approach as a means of discretising the space. More specifically, compact finite difference schemes are used to evaluate the spatial derivatives [26]. Thus, given u we are able to obtain the derivatives of u by solving a tridiagonal or pentadiagonal system.

5.1 Derivation of the High-Order Compact ADI Method for the Two-Parameter Mixed Derivative Equation

The range and domain is divided into a uniform mesh in each direction, in order to develop the high-order compact scheme, that is,

$$x_i = (i - 1)\Delta x, \quad i = 1, \dots, N_x, \quad y_j = (j - 1)\Delta y, \quad j = 1, \dots, N_y, \quad (5.1)$$

where Δx , Δy are the mesh sizes in the x- and y-direction respectively.

The two-dimensional two-parameter mixed derivative equation (4.1) can be written as,

$$\frac{u_{i,j}^{k+1} - u_{i,j}^k}{\Delta t} = \nu \left[(u_{xx})_{i,j}^k + (u_{yy})_{i,j}^k \right] + \alpha \left[\frac{(u_{xx})_{i,j}^{k+1} - (u_{xx})_{i,j}^k}{\Delta t} + \frac{(u_{yy})_{i,j}^{k+1} - (u_{yy})_{i,j}^k}{\Delta t} \right]. \quad (5.2)$$

We now take a half-step of (5.2) in the x-direction to obtain,

$$\frac{u_{i,j}^{k+\frac{1}{2}} - u_{i,j}^k}{\frac{1}{2}\Delta t} = \nu \left[(u_{xx})_{i,j}^{k+\frac{1}{2}} + (u_{yy})_{i,j}^k \right] + \alpha \left[\frac{(u_{xx})_{i,j}^{k+\frac{1}{2}} - (u_{xx})_{i,j}^k}{\frac{1}{2}\Delta t} + \frac{(u_{yy})_{i,j}^{k+\frac{1}{2}} - (u_{yy})_{i,j}^k}{\frac{1}{2}\Delta t} \right]. \quad (5.3)$$

Since we are taking half-steps in the x-direction only and no half-steps in the y-direction,

$$(u_{xx})_{i,j}^k = 0, \quad \text{and} \quad (u_{yy})_{i,j}^{k+\frac{1}{2}} = 0. \quad (5.4)$$

Therefore, in the x-direction we have,

$$\frac{u_{i,j}^{k+\frac{1}{2}} - u_{i,j}^k}{\frac{1}{2}\Delta t} = \nu \left[(u_{xx})_{i,j}^{k+\frac{1}{2}} + (u_{yy})_{i,j}^k \right] + \alpha \left[\frac{(u_{xx})_{i,j}^{k+\frac{1}{2}} - (u_{yy})_{i,j}^k}{\frac{1}{2}\Delta t} \right]. \quad (5.5)$$

Similarly taking a half-step in the y-direction of (5.2) results in,

$$\frac{u_{i,j}^{k+1} - u_{i,j}^{k+\frac{1}{2}}}{\frac{1}{2}\Delta t} = \nu \left[(u_{xx})_{i,j}^{k+\frac{1}{2}} + (u_{yy})_{i,j}^{k+1} \right] + \alpha \left[\frac{(u_{yy})_{i,j}^{k+1} - (u_{xx})_{i,j}^{k+\frac{1}{2}}}{\frac{1}{2}\Delta t} \right]. \quad (5.6)$$

We take the sixth-order compact formulas, developed by Chen and Liu [25] and also found in more detail in the paper by Gaitonde and Visbal [27], to approximate the derivatives in (5.5) and (5.6). The resulting formula is,

$$(u_{xx})_{,j} = \frac{1}{(\Delta x)^2} A^{-1} B u_{,j}, \quad (5.7)$$

where A and B are the $N_x \times N_x$ triangular sparse matrices and $u_{,j} = (u_{1,j}, u_{2,j}, \dots, u_{N_x,j})'$ is the solution of the j^{th} row.

Equation (5.7) is substituted into (5.5),

$$u_{,j}^{k+\frac{1}{2}} = u_{,j}^k + \frac{\Delta t \nu}{2} \left[\frac{1}{(\Delta x)^2} A^{-1} B u_{,j}^{k+\frac{1}{2}} + (u_{yy})_{,j}^k \right] + \alpha \left[\frac{1}{(\Delta x)^2} A^{-1} B u_{,j}^{k+\frac{1}{2}} - (u_{yy})_{,j}^k \right]. \quad (5.8)$$

Rearranging gives,

STAGE 1:

$$\left(I_x - \frac{1}{2}\nu \frac{\Delta t}{(\Delta x)^2} A^{-1} B - \alpha \frac{1}{(\Delta x)^2} A^{-1} B \right) u_{,j}^{k+\frac{1}{2}} = u_{,j}^k - \left(\alpha - \frac{\Delta t \nu}{2} \right) (u_{yy})_{,j}^k. \quad (5.9)$$

Similarly, we substitute the result of the sixth-order formulas,

$$(u_{yy})_{i,} = \frac{1}{(\Delta y)^2} C^{-1} D u_{i,}, \quad (5.10)$$

into (5.6) to obtain,

STAGE 2:

$$\left(I_y - \frac{1}{2}\nu \frac{\Delta t}{(\Delta y)^2} C^{-1} D - \alpha \frac{1}{(\Delta y)^2} C^{-1} D \right) u_{i,}^{k+1} = u_{i,}^{k+\frac{1}{2}} - \left(\alpha - \frac{\Delta t \nu}{2} \right) (u_{xx})_{i,}^{k+\frac{1}{2}}, \quad (5.11)$$

where I_x and I_y are the $N_x \times N_x$ and $N_y \times N_y$ identity matrices respectively.

5.2 Stability Analysis

Due to their high accuracy compactness (i.e. consuming less memory space) and better resolution for high frequency waves [26] the high-order compact difference methods have been employed in many contexts such as acoustics [28, 29, 30], computational electromagnetics [31, 32], oceanic applications [33, 34, 35] and many more. Much research has been conducted to obtain the appropriate formulae required and to show that the compact scheme has a smaller dispersive error in comparison to the same order explicit difference schemes [26, 36]. We will not provide an in depth discussion of this method but rather provide that which pertains to the solution of the mixed derivative equation under discussion. A vast amount of work has been done in this regard in the following articles [37, 38, 39, 40, 41, 42, 43, 44, 45].

We assume u is periodic in x and y as in [25] and therefore for a periodic problem for the sixth-order scheme A and B are,

$$A u_i = \beta u_{i-1} + u_i + \beta u_{i+1}, \quad (5.12)$$

$$B u_i = \frac{b}{4} (u_{i+2} - 2u_i + u_{i-2}) + a (u_{i+1} - 2u_i + u_{i-1}), \quad (5.13)$$

where β is a constant coefficient.

Let,

$$u_{i,j}^k = \epsilon^k e^{I(\omega_x i + \omega_y j)}, \quad I = \sqrt{-1}, \quad (5.14)$$

be the solution of u where the phase angles are represented by,

$$\omega_x = \frac{2\pi\Delta x}{l_x}, \quad \omega_y = \frac{2\pi\Delta y}{l_y},$$

where l_x and l_y represent the corresponding wavelengths. Substitute (5.14) into (5.12) and (5.13), with $\Delta y = 0$ since change is in the x -direction and y is kept constant to obtain,

$$A\epsilon^k e^{I\omega_x i} = \beta\epsilon^k e^{I\omega_x(i-1)} + \epsilon^k e^{I\omega_x i} + \beta\epsilon^k e^{I\omega_x(i+1)},$$

$$\begin{aligned} Ae^{I\omega_x i} &= \beta e^{I\omega_x i} e^{-I\omega_x} + e^{I\omega_x i} + \beta e^{I\omega_x i} e^{I\omega_x} \\ &= e^{I\omega_x i} (\beta e^{I\omega_x} + 1 + \beta e^{-I\omega_x}). \end{aligned}$$

Since $2 \cos x = e^{ix} + e^{-ix}$ we find that,

$$Ae^{I\omega_x i} = e^{I\omega_x i} (2\beta \cos \omega_x + 1). \quad (5.15)$$

Also,

$$B\epsilon^k e^{I\omega_x i} = \frac{b}{4} \left[\epsilon^k e^{I\omega_x(i+2)} - 2\epsilon^k e^{I\omega_x i} + \epsilon^k e^{I\omega_x(i-2)} + a(\epsilon^k e^{I\omega_x(i+1)} - 2\epsilon^k e^{I\omega_x i} + \epsilon^k e^{I\omega_x(i-1)}) \right]. \quad (5.16)$$

Similarly as for A, regrouping gives,

$$\begin{aligned} Be^{I\omega_x i} &= e^{I\omega_x i} \left[\frac{b}{4} (e^{2I\omega_x} - 2 + e^{-2I\omega_x}) + a(e^{I\omega_x} - 2 + e^{-I\omega_x}) \right] \\ &= e^{I\omega_x i} \left[\frac{b}{4} (2 \cos 2\omega_x - 2) + a(2 \cos \omega_x - 2) \right]. \end{aligned}$$

Since $\cos 2x = 1 - 2 \sin^2 x = 2 \cos^2 x - 1$ we obtain,

$$Be^{I\omega_x i} = e^{I\omega_x i} \left[(-b)(\sin^2 \omega_x) - (4a)(\sin^2 \frac{\omega_x}{2}) \right]. \quad (5.17)$$

Therefore we substitute the resulting A and B into (5.7) to obtain,

$$\begin{aligned} (u_{xx})_{ij}^{k+\frac{1}{2}} &= \frac{1}{(\Delta x)^2} A^{-1} B u_{ij}^{k+\frac{1}{2}} \\ &= \frac{u_{ij}^{k+\frac{1}{2}}}{(\Delta x)^2} \left[\frac{(-b)(\sin^2 \omega_x) - (4a)(\sin^2 \frac{\omega_x}{2})}{(2\beta \cos \omega_x + 1)} \right]. \end{aligned} \quad (5.18)$$

and similarly in the y-direction, with no change in the x-direction $\Delta x = 0$ and subsequently since $w_x = 0$,

$$C^{-1}D = \frac{(-b)(\sin^2 \omega_y) - (4a)(\sin^2 \frac{\omega_y}{2})}{(2\beta \cos \omega_y + 1)}. \quad (5.19)$$

Let,

$$\lambda_x = \frac{(-b)(\sin^2 \omega_x) - (4a)(\sin^2 \frac{\omega_x}{2})}{(2\beta \cos \omega_x + 1)}, \quad (5.20)$$

$$\lambda_y = \frac{(-b)(\sin^2 \omega_y) - (4a)(\sin^2 \frac{\omega_y}{2})}{(2\beta \cos \omega_y + 1)}, \quad (5.21)$$

$$m_x = \frac{1}{2} \frac{\nu \Delta t}{(\Delta x)^2}, \quad m_y = \frac{1}{2} \frac{\nu \Delta t}{(\Delta y)^2}, \quad (5.22)$$

$$n_x = \frac{\alpha}{(\Delta x)^2}, \quad n_y = \frac{\alpha}{(\Delta y)^2}. \quad (5.23)$$

Therefore equation (5.18) can be written as,

$$(u_{xx})_{i,j}^{k+\frac{1}{2}} = \frac{1}{(\Delta x)^2} A^{-1} B u_{i,j}^{k+\frac{1}{2}} = \frac{1}{(\Delta x)^2} \lambda_x u_{i,j}^{k+\frac{1}{2}}, \quad (5.24)$$

and similarly,

$$(u_{yy})_{i,j}^{k+1} = \frac{1}{(\Delta y)^2} C^{-1} D u_{i,j}^{k+1} = \frac{1}{(\Delta y)^2} \lambda_y u_{i,j}^{k+1}. \quad (5.25)$$

When substituting (5.20), (5.21), (5.22) and (5.23) into (5.5) we obtain,

$$u_{i,j}^{k+\frac{1}{2}} - u_{i,j}^k = \frac{\nu\Delta t}{2} \left[\frac{1}{(\Delta x)^2} \lambda_x u_{i,j}^{k+\frac{1}{2}} + \frac{1}{(\Delta y)^2} \lambda_y u_{i,j}^k \right] + \alpha \left[\frac{1}{(\Delta x)^2} \lambda_x u_{i,j}^{k+\frac{1}{2}} - \frac{1}{(\Delta y)^2} \lambda_y u_{i,j}^k \right],$$

which implies that,

$$\left(1 - \frac{1}{2} \frac{\nu\Delta t}{(\Delta x)^2} \lambda_x - \frac{\alpha}{(\Delta x)^2} \lambda_x \right) u_{i,j}^{k+\frac{1}{2}} = \left(1 + \frac{1}{2} \frac{\nu\Delta t}{(\Delta y)^2} \lambda_y - \frac{\alpha}{(\Delta y)^2} \lambda_y \right) u_{i,j}^k,$$

and therefore,

$$(1 - (n_x + m_x)\lambda_x) u_{i,j}^{k+\frac{1}{2}} = (1 - (n_y - m_y)\lambda_y) u_{i,j}^k. \quad (5.26)$$

Similarly by substituting (5.20), (5.21), (5.22) and (5.23) into (5.6) we find that,

$$(1 - (n_y + m_y)\lambda_y) u_{i,j}^{k+1} = (1 - (n_x - m_x)\lambda_x) u_{i,j}^{k+\frac{1}{2}}. \quad (5.27)$$

From (5.26) and (5.27) we see that the amplification factor is given by,

$$\begin{aligned} |\epsilon| &= \left| \frac{u_{i,j}^{k+1}}{u_{i,j}^{k+\frac{1}{2}}} \right| \cdot \left| \frac{u_{i,j}^{k+\frac{1}{2}}}{u_{i,j}^k} \right| \\ &= \left| \frac{1 - (n_x - m_x)\lambda_x}{1 - (n_y + m_y)\lambda_y} \right| \cdot \left| \frac{1 - (n_y - m_y)\lambda_y}{1 - (n_x + m_x)\lambda_x} \right|. \end{aligned} \quad (5.28)$$

Moreover,

$$\begin{aligned} |\epsilon| &= \left| \frac{1 - \frac{1}{(\Delta x)^2} \left(\alpha - \frac{\nu\Delta t}{2} \right) \lambda_x}{1 - \frac{1}{(\Delta y)^2} \left(\alpha + \frac{\nu\Delta t}{2} \right) \lambda_y} \right| \cdot \left| \frac{1 - \frac{1}{(\Delta y)^2} \left(\alpha - \frac{\nu\Delta t}{2} \right) \lambda_y}{1 - \frac{1}{(\Delta x)^2} \left(\alpha + \frac{\nu\Delta t}{2} \right) \lambda_x} \right| \\ &= \left| \frac{1 + \frac{1}{(\Delta x)^2} \left(\frac{\nu\Delta t}{2} - \alpha \right) \lambda_x}{1 - \frac{1}{(\Delta y)^2} \left(\frac{\nu\Delta t}{2} + \alpha \right) \lambda_y} \right| \cdot \left| \frac{1 + \frac{1}{(\Delta y)^2} \left(\frac{\nu\Delta t}{2} - \alpha \right) \lambda_y}{1 - \frac{1}{(\Delta x)^2} \left(\frac{\nu\Delta t}{2} + \alpha \right) \lambda_x} \right|. \end{aligned}$$

Therefore, since in our calculations, $\frac{1}{\Delta x}^2 = \frac{1}{\Delta y}^2$ and $\lambda_x, \lambda_y \leq 0$, our methods (5.5) and (5.6) are stable under the conditions where $\alpha, \nu > 0$.

5.3 Numerical Analysis and Results

In this section, the solutions of the two-stage method derived in the previous section, is analysed. The equations in question are the two stages,

STAGE 1:

$$\left(I_x - \frac{1}{2}\nu \frac{\Delta t}{(\Delta x)^2} A^{-1}B - \alpha \frac{1}{(\Delta x)^2} A^{-1}B \right) u_{i,j}^{k+\frac{1}{2}} = u_{i,j}^k - \left(\alpha - \frac{\Delta t\nu}{2} \right) (u_{yy})_{i,j}^k, \quad (5.29)$$

STAGE 2:

$$\left(I_y - \frac{1}{2}\nu \frac{\Delta t}{(\Delta y)^2} C^{-1}D - \alpha \frac{1}{(\Delta y)^2} C^{-1}D \right) u_{i,j}^{k+1} = u_{i,j}^{k+\frac{1}{2}} - \left(\alpha - \frac{\Delta t\nu}{2} \right) (u_{xx})_{i,j}^{k+\frac{1}{2}}. \quad (5.30)$$

We discretise the intervals $x \in [k, l]$ and $y \in [c, d]$ by sub-dividing them into N equidistant intervals termed Δx and Δy . In this case we have chosen these step sizes to be of equal size. Thus, given that $0 = x_0 < x_1 < x_2 < \dots < x_{N-1} < x_N$ we define $\Delta x = x_{i+1} - x_i$ - in a similar fashion we have that $\Delta y = y_{j+1} - y_j$. At interior nodes we use the formula from [26] which provides the approximation of the second derivative in terms of the space variable x as follows,

$$\beta u_{i-1}'' + u_i'' + \beta u_{i+1}'' = b \frac{u_{i+2} - 2u_i + u_{i-2}}{4\Delta x^2} + a \frac{u_{i+1} - 2u_i + u_{i-1}}{\Delta x^2}. \quad (5.31)$$

This provides a β -family of sixth-order accurate schemes when $a = 12/11$, $b = 3/11$ and $\beta = 2/11$. In our case the near boundary nodes are obtained via the zero-shear boundary conditions given by (4.40). In this manner we obtain the sixth-order formula,

$$(u_{xx})_j = \frac{1}{\Delta x^2} A^{-1} B u_{\cdot,j}, \quad (5.32)$$

where A and B are $N \times N$ sparse matrices and $u_{\cdot,j} = (u_{1,j}, u_{2,j}, \dots, u_{N,j})'$ is the solution vector at the j th row. We define these coefficient matrices as follows,

$$A = \begin{bmatrix} 1 & 2\beta & 0 & 0 & \dots & 0 & 0 & 0 & 0 \\ \beta & 1 & \beta & 0 & \dots & 0 & 0 & 0 & 0 \\ 0 & \beta & 1 & \beta & \dots & 0 & 0 & 0 & 0 \\ \vdots & \ddots & \ddots & \ddots & \ddots & \ddots & \ddots & \ddots & \vdots \\ 0 & 0 & 0 & 0 & \dots & 0 & \beta & 1 & \beta \\ 0 & 0 & 0 & 0 & \dots & 0 & 0 & 2\beta & 1 \end{bmatrix},$$

$$B = \begin{bmatrix} -\frac{b}{2} - 2a & 2a & \frac{b}{2} & 0 & 0 & 0 & \cdots & 0 & 0 & 0 & 0 & 0 & 0 \\ a & -\frac{b}{4} - 2a & a & \frac{b}{4} & 0 & 0 & \cdots & 0 & 0 & 0 & 0 & 0 & 0 \\ \frac{b}{4} & a & -\frac{b}{2} - 2a & a & \frac{b}{4} & 0 & \cdots & 0 & 0 & 0 & 0 & 0 & 0 \\ \vdots & \ddots & \ddots & \ddots & \ddots & \ddots & \ddots & \ddots & \ddots & \ddots & \ddots & \ddots & \vdots \\ 0 & 0 & 0 & 0 & 0 & 0 & \cdots & 0 & \frac{b}{4} & a & -\frac{b}{2} - 2a & a & \frac{b}{4} \\ 0 & 0 & 0 & 0 & 0 & 0 & \cdots & 0 & 0 & \frac{b}{4} & a & -\frac{b}{4} - 2a & a \\ 0 & 0 & 0 & 0 & 0 & 0 & \cdots & 0 & 0 & 0 & \frac{b}{2} & 2a & -\frac{b}{2} - 2a \end{bmatrix}. \quad (5.33)$$

Similarly we have,

$$(u_{yy})_i = \frac{1}{\Delta y^2} C^{-1} D u_i, \quad (5.34)$$

where $C = A$ and $D = B$ are $N \times N$ sparse matrices and $u_i = (u_{i,1}, u_{i,2}, \dots, u_{i,N})'$ is the solution vector at the i th column.

Eliminating $(u_{xx})_{i,j}$ and $(u_{yy})_{i,j}$ from the stages (5.30) and (5.29) respectively, with the use of equations (5.32) and (5.34) we obtain the stages,

STAGE 1:

$$\left(I_x - \frac{1}{2} \nu \frac{\Delta t}{(\Delta x)^2} A^{-1} B - \alpha \frac{1}{(\Delta x)^2} A^{-1} B \right) u_{i,j}^{k+\frac{1}{2}} = \left(I_x - \left(\frac{\alpha}{(\Delta y^2)} - \frac{\Delta t \nu}{2(\Delta y^2)} \right) C^{-1} D \right) u_{i,j}^k, \quad (5.35)$$

STAGE 2:

$$\left(I_y - \frac{1}{2} \nu \frac{\Delta t}{(\Delta y)^2} C^{-1} D - \alpha \frac{1}{(\Delta y)^2} C^{-1} D \right) u_{i,j}^{k+1} = \left(I_y - \left(\frac{\alpha}{(\Delta x^2)} - \frac{\Delta t \nu}{2(\Delta x^2)} \right) A^{-1} B \right) u_{i,j}^{k+\frac{1}{2}}. \quad (5.36)$$

The above scheme has a truncation error of $O((\Delta t)^2, (\Delta x)^6, (\Delta y)^6)$. Given that the inverse matrices A^{-1} and C^{-1} are time-independent matrices they only need to be calculated once and can be stored before the time-marching allowing for computational efficiency. In a similar fashion the domain $[0, T]$ is sub-divided into M intervals of equal length, Δt , through which the scheme iterates. The system iterates with step-sizes $\Delta x = 0.1$, $\Delta t = 0.0001$ such that $\beta = \Delta t / \Delta x^2 = 0.01$ and will iterate until $t_m + \Delta t = T$, i.e. for $M = T / \Delta t$ steps.

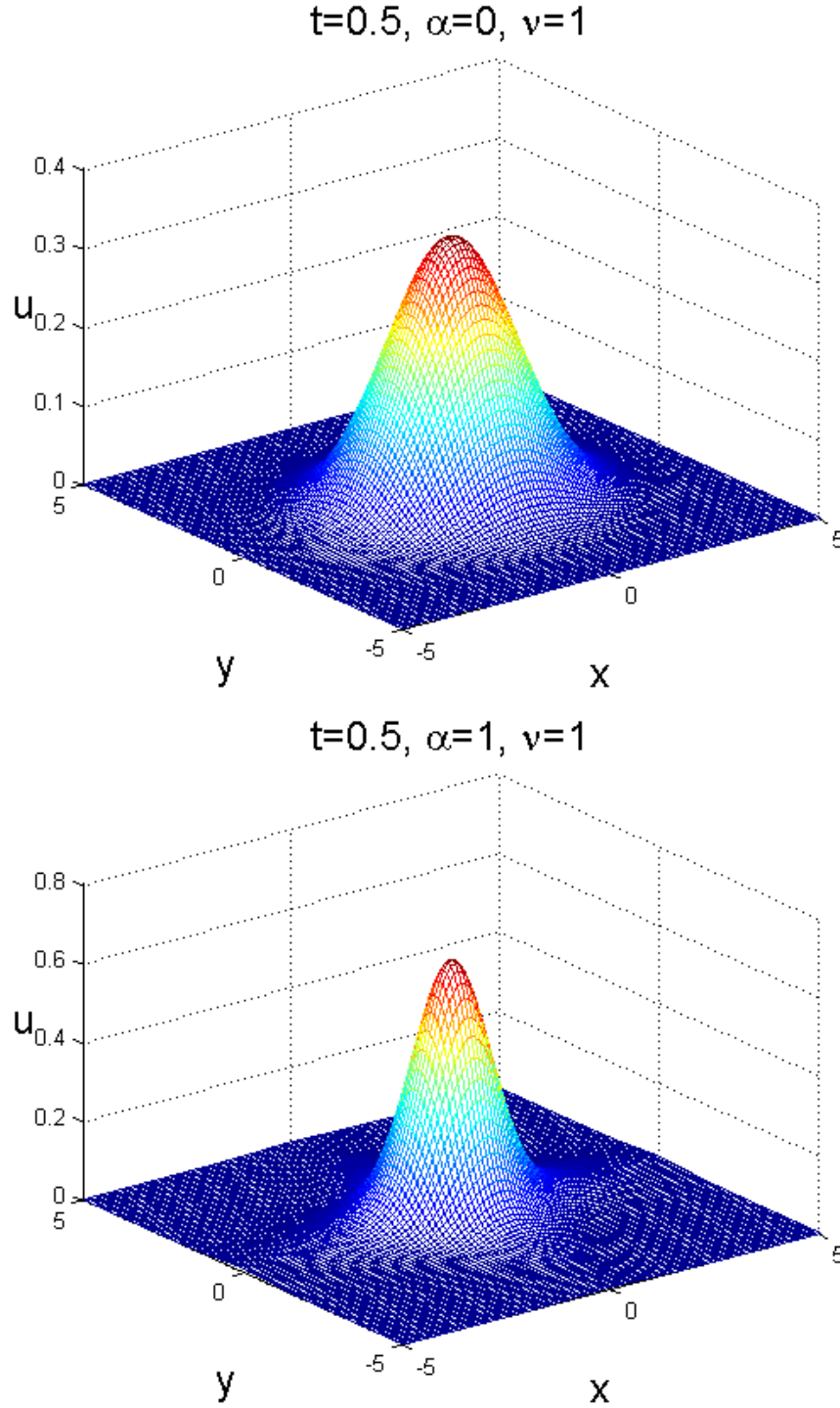


Figure 5.1: Plot of $u(x, y, t)$ of the Compact ADI method at $\alpha = 0$ and for $\nu = 1$ (top) and $\alpha = 1$ and $\nu = 1$ (bottom), $N=100$.

The results presented in Figure 5.1, are for the same parameter values as in the previous section, except here we are implementing a scheme of higher accuracy due to the higher order method adopted. The initial curve used is the same as before and given by $u^0(x_i, y_j) = \exp(-x_i^2 - y_j^2)$.

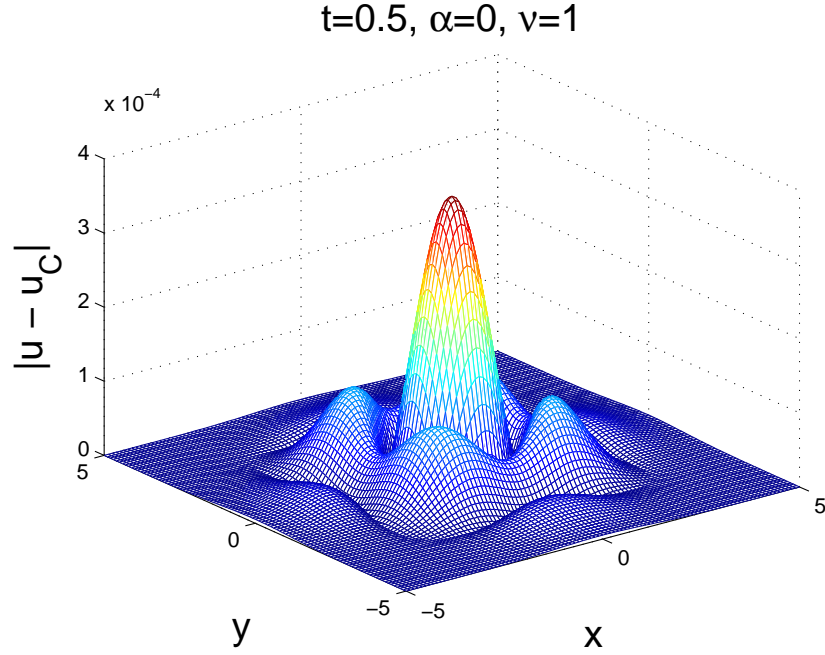


Figure 5.2: Plot of the absolute error between the numerical solution obtained via the ADI method and the numerical solution obtained via the compact ADI method for $\Delta t = 0.05$ and $N = 100$.

5.4 Comparative Study between the ADI and Compact ADI Methods

For completeness in our consideration of the accuracy of our numerical solutions we consider the log of the absolute error between the numerical solution obtained via the ADI method and the numerical solution obtained via the compact ADI method. In Figure 5.3 we have plotted the $\text{Log}|\mathbf{u} - \mathbf{u}_C|$ where \mathbf{u}_C is the numerical solution obtained via the compact ADI method. The order of the error among the numerical solutions is approximately $O(10^{-7})$, allowing for an accuracy close to 7 decimal places between the two solutions.

We then consider the L_∞ norm (or more specifically the maximum norm) of a vector of the difference between the numerical solution obtained via the ADI method and the numerical solution obtained via the compact ADI method. The maximum norm of the error, defined as $\|A\|_\infty = \max_{x \neq 0} \left(\frac{\max_{1 \leq i \leq n} |(Ax)_i|}{\max_{1 \leq i \leq n} |(x)_i|} \right)$ where $A = \mathbf{u} - \mathbf{u}_C$, will be considered over a range of $\varphi = \Delta t / \Delta x^2$ values as a means of ascertaining the degree to which the choices of Δt and Δx influence its value. This range of values for φ is obtained by considering $\Delta t = 0.0001$ and $\Delta x = 0.01, 0.02, 0.05, 0.08, 0.1, 0.12, 0.15, 0.2$.

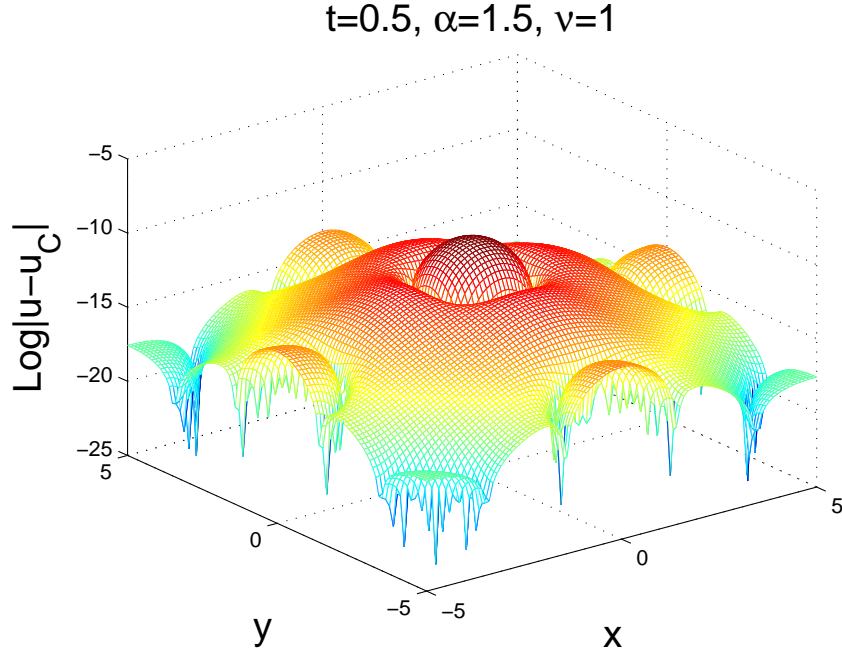


Figure 5.3: Plot of the log of the absolute error between the numerical solution obtained via the ADI method and the numerical solution obtained via the compact ADI method for $\Delta t = 0.05$ and $N = 100$.

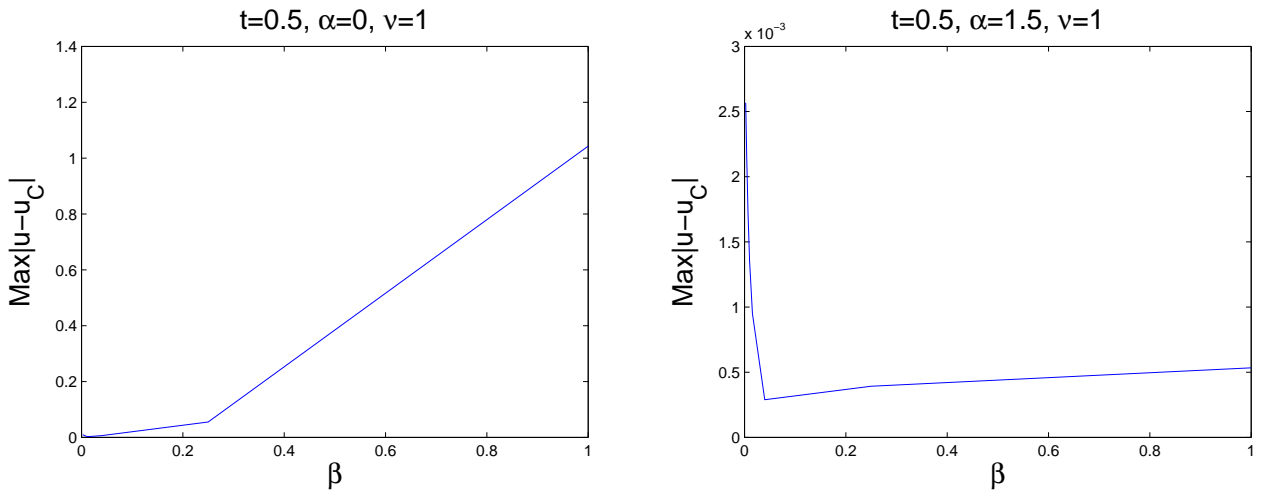


Figure 5.4: Plot of the infinity norm of the numerical solution obtained via the ADI method and the numerical solution obtained via the compact ADI method for $\Delta t = 0.05$ and $N = 100$.

In Figure 5.4 we have plotted two cases in which the infinity norm was considered for $\nu = 1$, namely: $\alpha = 0$ and $\alpha = 1.5$. We have also considered values of α which lie in between these two values. It was found - and is more clearly visible when comparing the plots in Figure 5.4 - that the value of α seems to affect the order of the infinity norm obtained as φ increases. We find that we maintain a lower L_∞ norm for larger values of φ as α increases, whereas the smaller α , the more severe the impact of a change in φ is found to be. This seems to indicate that smaller values of α increase the differences between the two methods as φ increases. In considering the actual numerical solutions for $\alpha = 0$ and $\nu = 1$, we find that it is the compact ADI solution which diverges and produces nonsensical results. This seems to indicate that for small α the compact ADI scheme is more likely to become unstable if inappropriate values of Δx and Δt are chosen.

5.5 Physical Interpretation of Results

Here we take a look at the behaviour of the resulting solutions of the high-order method for different values of the two parameters in the mixed derivative equation (1.9). It is to be noted that the choice of values of α and ν are to demonstrate the numerical effects of the solutions.

In order to display the effects of the viscosity parameter ν without the effects of viscoelasticity, the parameter ν is varied for values, $\nu = 3, 5, 7$ while $\alpha = 0$, in Figure 5.5 and Figure 5.6.

It can be seen, as before, that as ν increases, the profile broadens, showing the progression of diffusion in the solution. As ν increases the Reynolds number becomes very small, given that $\nu \gg UL$ and therefore $Re \ll 1$, which leads to the solution exhibiting slow viscous flow.

Introducing the effects of the viscoelasticity, for the values of $\alpha = 1, 3, 5$ while keeping the viscosity constant at $\nu = 7$, we see the effects of diffusion being counteracted by a gradual increase in the profile height of the solution in Figure 5.7 and Figure 5.8.

At $\alpha = 5$ and $\nu = 7$ we see a similar disturbance along the boundaries at $\frac{\partial u}{\partial x} \approx 0$ and $\frac{\partial u}{\partial y} \approx 0$. As such when $Re = \frac{UL}{\nu} \gg \frac{L^2}{\alpha}$, then the viscoelastic effects are important and evident in the behaviour of the solution.

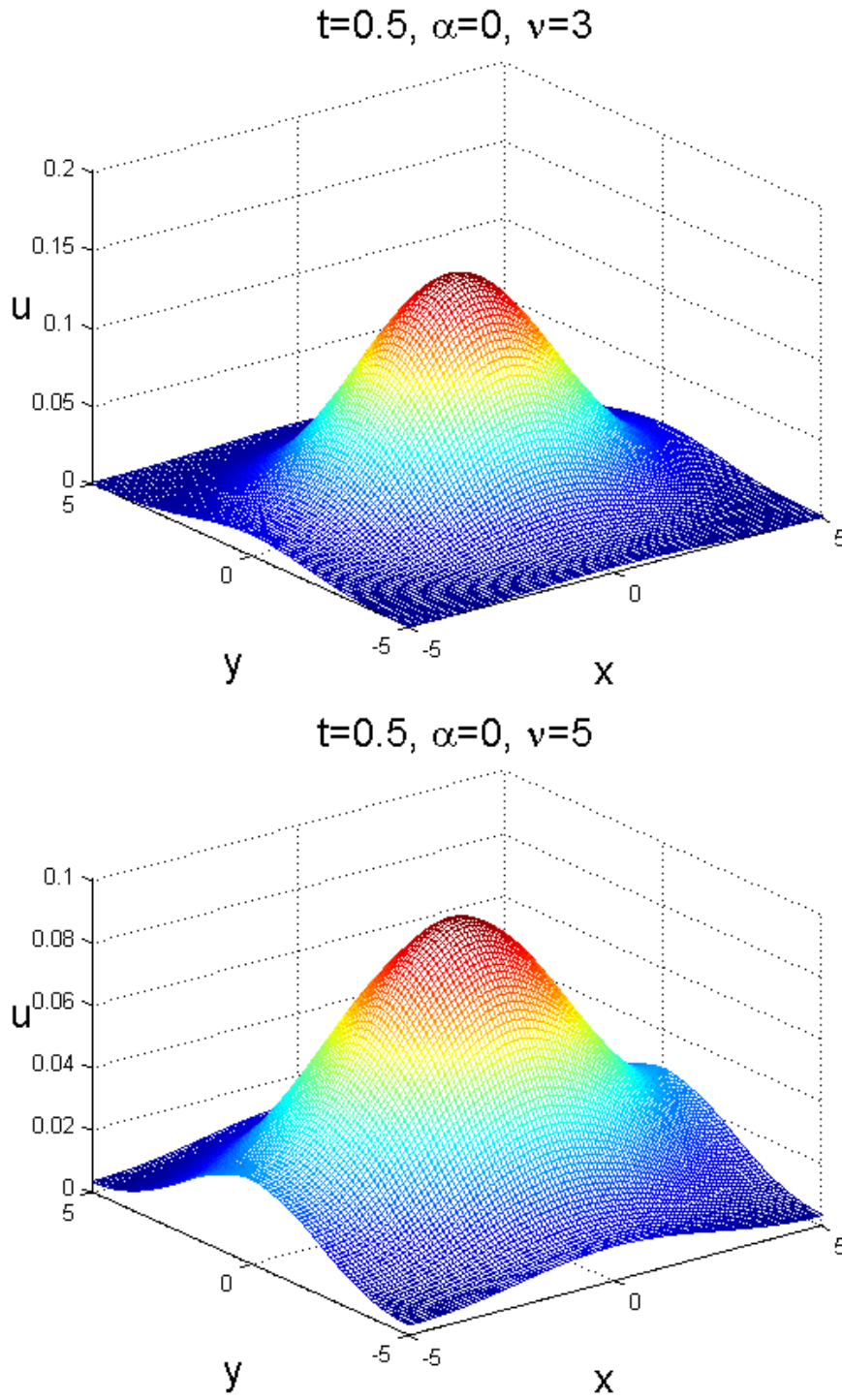


Figure 5.5: Plot of $u(x,y,t)$ displaying diffusion effects of the Compact ADI method at $\alpha = 0$ and $\nu = 3$ (top) and for $\alpha = 0$ and $\nu = 5$ (bottom).

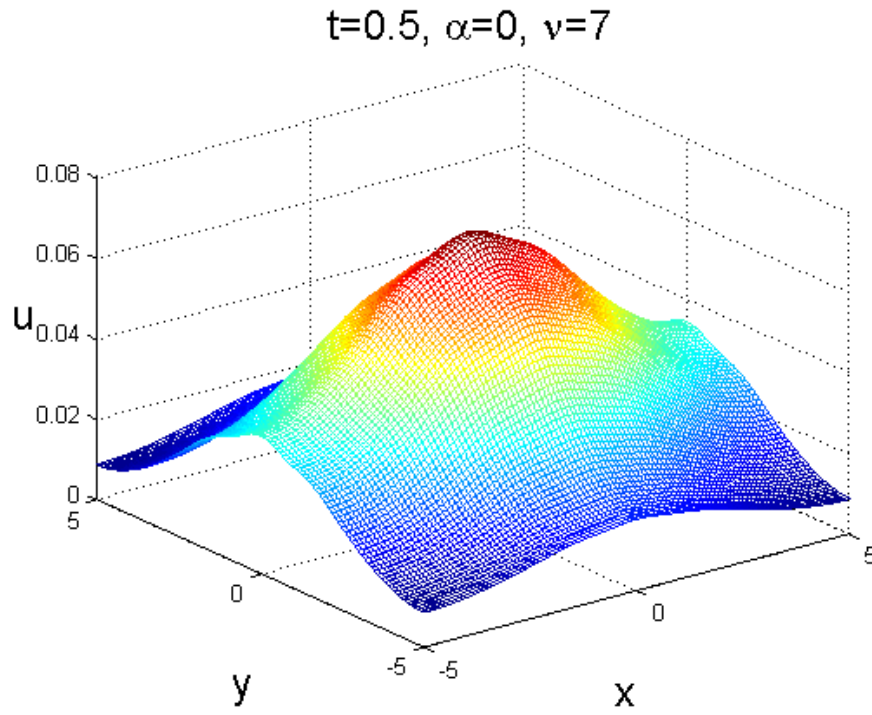


Figure 5.6: Plot of $u(x,y,t)$ displaying diffusion effects of the Compact ADI method at $\alpha = 0$ and $\nu = 7$.

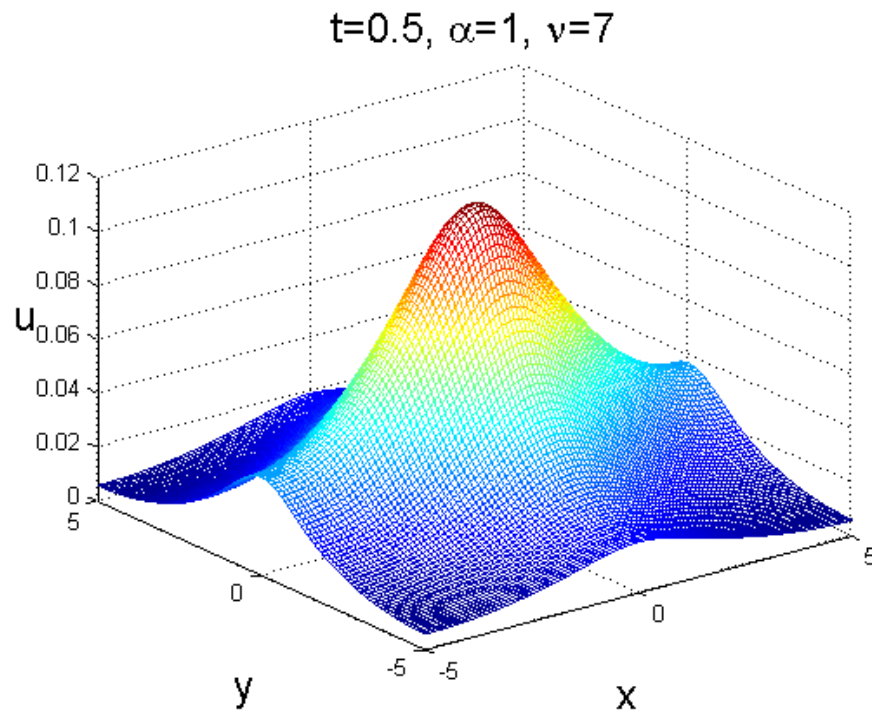


Figure 5.7: Plot of $u(x,y,t)$ displaying viscoelastic effects of the Compact ADI method at $\alpha = 1$ and $\nu = 7$.

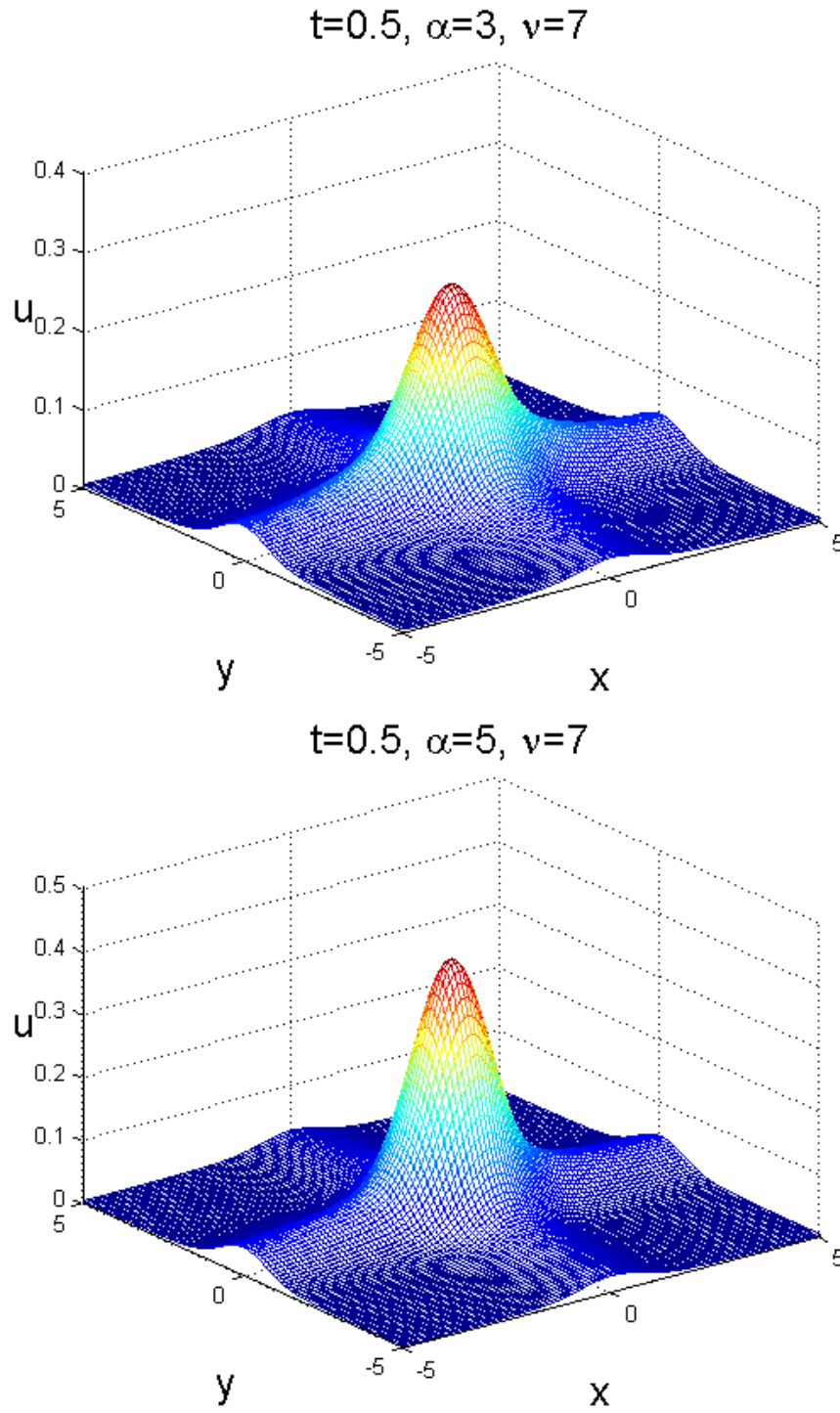


Figure 5.8: Plot of $u(x, y, t)$ displaying viscoelastic effects for $\alpha = 3$ and $\nu = 7$ (top) and for $\alpha = 5$ and $\nu = 7$ (bottom) .

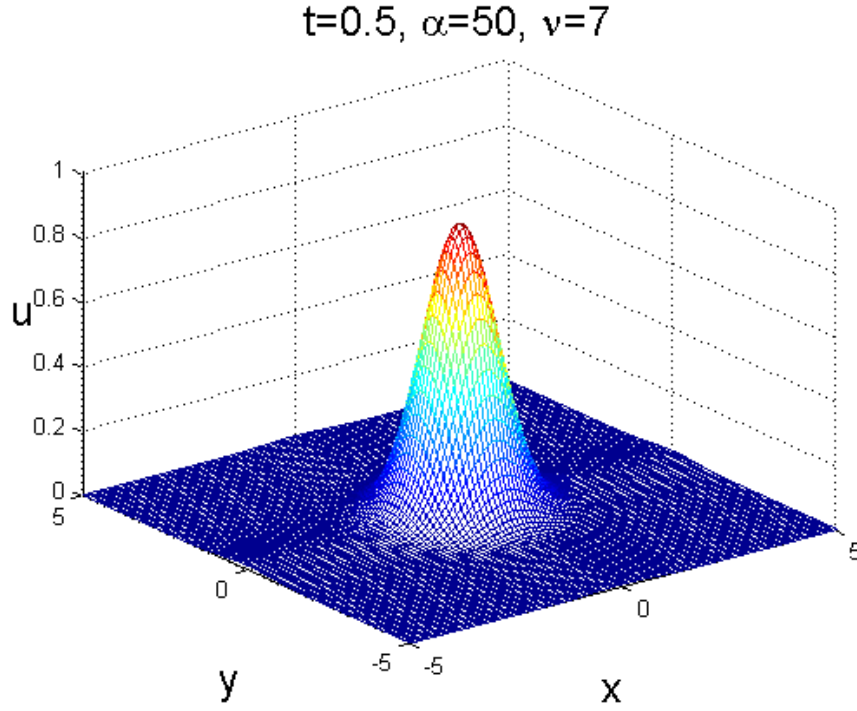


Figure 5.9: Plot of $u(x, y, t)$ displaying viscoelastic effects of the Compact ADI method at $\alpha = 50$ and $\nu = 7$.

Continuously increasing α above the value of ν , as displayed in Figure 5.9, shows the effects of diffusion to be negligible given that the profile height continues to increase without much broadening of the solution. The behaviour of the results are consistent, in general, with that of the previous chapter. However, with this high-order compact ADI method, we see for $\alpha > \nu$ and at high values of α and ν , the solutions are very consistent with the shape of the initial solution, exhibiting more sensible results than previously seen in Figure 4.7.

Chapter 6

Conclusion

We utilized numerical methods that have already been implemented on equations that model unidirectional flow in a viscoelastic fluid to analyse our parabolic mixed derivative diffusion equation (1.9). This exercise as well as the application and analysis of the Fourier and Laplace transform solutions on our two-parameter parabolic mixed derivative diffusion equation assisted in clarifying the behavioural expectations of the equation in the following chapters. Fourier and Laplace transform solutions of our mixed derivative diffusion equation reveals very consistent results with that previously dealt with by Momoniat [1] and Momoniat, McIntyre and Ravindran [9].

The one-dimensional parabolic mixed derivative diffusion equation was then extended to the two-dimensional analog. This was derived and numerically solved using the Crank-Nicholson method and implemented via the Peaceman-Rachford Alternating Direction Implicit Method.

An analysis of our two-parameter one-dimensional parabolic mixed derivative equation using the von Neumann stability analysis revealed a stable solution under the conditions where $\alpha, \nu > 0$. The results showed oscillatory behaviour for values of $\alpha \ll 0$ whereas solutions with $\alpha \geq 0$ rapidly decay to zero. The divergent nature of the solution at values of $\alpha \ll 0$ is numerically implemented and graphically represented in Figure 3.3. This behaviour is as expected from the finding of the analytical stability analysis.

The behaviour of the resulting solutions were investigated for different values of viscosity, ν and viscoelasticity, α , to show the evident effects of inertia, viscous flow and diffusion. In the absence of viscoelastic effects and only the presence of viscosity, the solution is shown to exhibit pure diffusion. When the effects of viscoelasticity is introduced back into the solution, with a constant viscosity of the fluid, the diffusion effects are counteracted by the narrowing and lengthening of the profile height as the viscoelastic parameter is increased.

Increasing the α to values very close to that of ν , that is, the ratio, we see the profile sharpens drastically. Also, very evident, is the disturbances caused along the boundaries of the solution at $\frac{\partial u}{\partial x} \approx 0$ and $\frac{\partial u}{\partial y} \approx 0$.

As the value of α is increased above ν , for large values of α and ν , that is, $D = \frac{\nu}{\alpha} \ll 1$, the disturbances along the boundaries become very large causing the solution to diverge from the stable parabolic shape of the initial solution. The behaviour of the solutions is summarised in the Table 6.1.

	Parameter Values	Behaviour of the Solution
1.	$\alpha = 0, \nu = 2, 4, 6, 9$ and $Re \ll 1$ with $UL \ll \nu$	The fluid exhibits slow viscous flow. Diffusion effects on the profile are dominant
2.	$\alpha = 1, 2, 3, 5, \nu = 9$ and $Re \gg \frac{L^2}{\alpha}$	Domination of viscoelastic effects and increased profile height
3.	$\alpha > \nu, D = \frac{\nu}{\alpha} \ll 1$	Negligible effects of diffusion. Solution shape diverges from initial solution.

Table 6.1: Summary of the behaviour of the parameters as a result of the general ADI numerical solutions

The two-dimensional parabolic mixed derivative diffusion equation was also analysed using a high-order Peaceman-Rachford implementation, generally referred to in the text as the compact ADI method. The resulting numerical method was shown to be stable in the case where $\alpha, \nu > 0$.

An error analysis, was executed in order to make a comparison of the accuracy of the sixth-order accurate compact ADI method and the Peaceman-Rachford ADI method. The log of the absolute error between the numerical solution of the ADI method and the numerical solution of the compact ADI method reveals an order of error between the solutions of approximately $O(10^{-7})$ allowing for an accuracy close to 7 decimal places. The infinity norm, L_∞ norm, of the numerical solutions, reveals that the larger the values of α , the smaller the differences between the two methods. Whereas for smaller values of α , we find that the compact ADI method is particularly sensitive to values chosen for Δx and Δt .

As is the case for the ADI method, the compact ADI method displays dominant diffusion effects when considering values of ν without considering the effects of viscoelasticity, α . Also holding ν constant while varying the values of α , causes the viscoelastic effects to counteract the diffusion effects and subsequently bring the graph to a sensible shape. As α is increased there is a similar lifting along the boundaries, $\frac{\partial u}{\partial x}$ and $\frac{\partial u}{\partial y}$, just as in the case of the general ADI method. Therefore the results of the general ADI method are shown to be

consistent with that of the compact ADI method.

However, we also see that for high values of α and ν for $\alpha > \nu$, the lifting of the boundaries are not out of control to the point of causing a non-sensible shape of the solution. Instead the profile of the solutions of the compact ADI method is consistent with the profile shape of the initial solution unlike the solutions obtained using the general ADI method. The behaviour of the solutions is summarised in the Table 6.2.

	Parameter Values	Behaviour of the Solution
1.	$\alpha = 0, \nu = 3, 5, 7$ and $Re \ll 1$ with $UL \ll \nu$	The fluid exhibits slow viscous flow. Diffusion effects on the profile are dominant
2.	$\alpha = 1, 3, 5, \nu = 7$ and $Re \gg \frac{L^2}{\alpha}$	Domination of viscoelastic effects and increased profile height
3.	$\alpha \gg \nu, D = \frac{\nu}{\alpha} \ll 1$	Negligible effects of diffusion. Solution shape is consistent with initial solution.

Table 6.2: Summary of the behaviour of the parameters as a result of the compact ADI numerical solutions

The implementation of the one-dimensional two-parameter mixed derivative diffusion equation produced consistent results with that of its two-dimensional analog for both the general and compact ADI implementations. The behaviour of these solutions proved unstable, analytically and numerically, for the case when $\alpha \ll 0$ and $\nu > 0$. The Fourier and Laplace transform solutions were consistent with the results for the implementations that followed.

The two-parameter mixed derivative diffusion equation has not been considered before. Moreover, the 6th order numerical solutions have not been previously considered for such an equation, and thus the high-order compact ADI implementation has proven to present more accurate solutions for the behavioural analysis of our mixed derivative diffusion equation.

Bibliography

- [1] E. Momoniat, *A Point Source Solution for a Unidirectional Flow of a Viscoelastic Fluid*, Phys. Lett. A, (2008), **372**, 4041–4044.
- [2] C. Cattaneo, *Sulla Conduzione del calore*, Atti. Sem. Mat. Fis. Univ. Mod., **3**, (1948), 83–100.
- [3] E. Momoniat, *On the Diffusion of a Point Source Modelled by a Mixed Derivative Equation*, Phys. A, **387**, (2008), 2427–2432.
- [4] C. Wafo Soh, *Comment on: A Point Source Solution for a Unidirectional Flow of a Viscoelastic Fluid*, Phys. Lett. A, **374**, (2010), 2098–2100.
- [5] E. Momoniat and C. Harley, *Peaceman-Rachford ADI Scheme for the Two Dimensional Flow of a Second-Grade Fluid*, Amer. Instit. Phys. Conf. Proc., **1168**, (2009), 1343–1346.
- [6] R. S. Rivlin and J. L. Ericksen, *Stress Deformation for Isotropic Materials*, J. Rat. Mech. Anal., (1955), **4**, 323–333.
- [7] K. R. Rajagopal, *A Note on Unsteady Unidirectional Flows of a Non-Newtonian Fluid*, Int. J. Non-Lin. Mech., **17**, (1982), 369–373.
- [8] T. Hayat, M. Khan, A. M. Siddiqui and S. Asghar, *Transient Flows of a Second Grade Fluid*, Int. J. Non-Lin. Mech., **39**, (2004), 1621–1633.
- [9] E. Momoniat, R. McIntyre and R. Ravindran, *Numerical Inversion of a Laplace Transform Solution of a Diffusion Equation with a Mixed Derivative Term*, Appl. Math. Comput., **209**, (2009), 222–229.
- [10] J. Crank, *The Mathematics of Diffusion*, Oxford, Clarendon, (1970).
- [11] C. Cattaneo, *A Form of Heat Conduction Equation which Eliminates the Paradox of Instantaneous Propagation*, Compte Rendus., **247**, (1958), 431–433.
- [12] E. Momoniat, *A Comparison of Diffusion Modelled by Two Mixed Derivative Equations*, Mod. Phys. Lett. B, **22**, (2008), 2709–2713.

- [13] V. Girault and L. R. Scott *Analysis of a Two-Dimensional Grade-Two Fluid Model with a Tangential Boundary Condition*, J. Math. Pures Appl. , **78**, (1999), 981–1011.
- [14] I-Chung Liu, *Unsteady Unidirectional MHD Flows of a non-Newtonian Fluid Saturated in a Porous Medium*, J. Chin. Inst. Eng., **28**, (2005), 569–578.
- [15] R. A. Damseh, A. S. Shatnawi, A. J. Chamkha and H. M. Duwairi, *Transient Mixed Convection Flow of a Second-Grade Visco-Elastic Fluid over a Vertical Surface*, Nonlin. Anal. Mod. Contr., (2008), **13**, 169–179.
- [16] D. J. Acheson, *Elementary Fluid Dynamics*, Oxf. Appl. Math. Comp. Sci. Ser., New York, (1990).
- [17] G. K. Batchelor, *An Introduction to Fluid Dynamics*, Cambridge University Press, New York, (1967).
- [18] R. P. Chhabra and J.F. Richardson *Non-Newtonian Flow and Applied Rheology: Engineering Applications*, Elsevier Ltd, Oxford, (2008).
- [19] R. P. Chhabra and J.F. Richardson *Non-Newtonian Flow in the Process Industries, Fundamentals and Engineering Applications*, Butterworth-Heinemann, Oxford, (1999).
- [20] K. Weissenberg, *A continuum theory of rheological phenomena*, Nat., (1947), **159**, 310–311.
- [21] K. S. Crump, *Numerical Inversion of Laplace Transforms using a Fourier Series Approximation*, J. Assoc. Comp. Mach., **23**, (1976), 89–96.
- [22] R. F. Warming and B. J. Hyett, *The Modified Equation Approach to the Stability and Accuracy Analysis of Finite-Difference Methods*, J. Comp. Phys., (2009), **14**, (1974), 159–179.
- [23] J. Crank and E. Nicholson, *A Practical Method for Numerical Evaluation of Solutions of Partial Differential Equations of the Heat Conduction Type*, Proc. Camb. Phil. Soc., **43**, (1947) , 50–67.
- [24] D. W. Peaceman and H. H. Rachford, *The Numerical Solution of Parabolic and Elliptic Differential Equations*, J. Soc. Indust. Appl. Math., **3**, (1955), 28–41.
- [25] J. Li, Y. Chen and G. Liu, *High-Order Compact ADI Methods for Parabolic Equations*, Comp. Math. Appl., **52**, (2006) , 1343–1356.
- [26] S. K. Lele, *Compact Finite Difference Schemes with Spectral-like Resolution*, J. Comp. Phys., **103**, (1992) , 16–42.
- [27] D.V. Gaitonde and M.R. Visbal, *High-Order Schemes for Navier-Stokes Equations: Algorithms and Implementation into FDL3DI*, Technical Report AFRL-VA-WP-TR-1998-3060, Air Force Research Laboratory, Wright-Patterson AFB, OH, (1998).

- [28] R. Hixon and E. Turke;, *Compact implicit MacCormack-type schemes with high accuracy*, J. Comp. Phys., **158**, 51-70, (2000).
- [29] F.Q. Hu, M.Y. Hussaini and J.L. Manthey, *Low-dissipation and low- dispersion Runge-Kutta schemes for computational acoustics*, J. Comp. Phys., **124**, 177-191, (1996).
- [30] C.K.W. Tam and J.C. Webb, *Dispersion-relation-preserving finite difference schemes for computational acoustics*, J. Comp. Phys., **107**, 262-281, (1993).
- [31] J.S. Shang, *High-order compact-difference schemes for time- dependent Maxwell equations*, J. Comp. Phys., **153**, 312-333, (1999).
- [32] J. Li and Y. Chen, *High-order compact schemes for dispersive media*, Elect. Lett., **40**, 853-855, (2004).
- [33] I.M. Navon and H.A. Riphagen, *An implicit compact fourth order algorithm for solving the shallow-water equations in conservation-law form*, Month. Weath. Rev., **107**, 1107-1127, (1979).
- [34] I.M. Navon and H.A. Riphagen, *SHALL4 - An implicit compact fourth-order Fortran program for solving the shallow-water equations in conservation-law form*, Comp. Geosci., **12**, 129-150, (1986).
- [35] P.C. Chu and C. Fan, *A three-point combined compact difference scheme*, J. Comp. Phys., **140**, 370-399, (1998).
- [36] J. Li and M.R Visbal, *High-order compact schemes for nonlinear dispersive waves*, J. Sci. Comp., **26**, 1-23, (2006).
- [37] S. Abarbanel, A. Ditzkowski and B. Gustafsson, *On error bounds of finite difference approximations to partial differential equations - temporal behaviour and rate of convergence*, J. Sci. Comp., **15**, 79-116, (2000).
- [38] M.H. Carpenter, D. Gottlieb and S. Abarbanel, *Time-stable boundary conditions for finite-difference schemes solving hyperbolic systems: Methodology and application to high-order compact system*, J. Comp. Phys., **111**, 220-236, (1994).
- [39] M.H. Carpenter, D. Gottlieb and S. Abarbanel, *Stable and accurate boundary treatments for compact high order finite difference schemes*, Appl. Numer. Math., **12**, 55-87, (1993).
- [40] Y. Adam, *Highly accurate compact implicit methods and boundary conditions*, J. Comp. Phys., **24**, 10-22, (1977).
- [41] W.F. Spitz and G.F. Carey, *Extension of high order compact schemes to time dependent problems*, Numer. Meth. Part. Diff. Eqn., **17**, 657-672, (2001).

- [42] W. Dai and R. Nassar, *Compact ADI method for solving parabolic differential equations*, Numer. Meth. Part. Diff. Eqn., **18**, 129-142, (2002).
- [43] W. Liao, J. Zhu and A.Q.M. Khaliq, *An efficient high-order algorithm for solving systems of reaction-diffusion equations*, Numer. Meth. Part. Diff. Eqn., **18**, 340-354, (2002).
- [44] S. Karaa and J. Zhang, *High order ADI method for solving unsteady convection-diffusion problems*, J. Comp. Phys., **198**, 1-9, (2004).
- [45] K. Mattsson and J. Nordstrom, *Summation by parts operators for finite difference approximations of second derivatives*, J. Comp. Phys., **199**, 503-540, (2004).